da allegare (in pdf) al PROOF dell'articolo:

Link sito dell'editore:
https://www.sciencedirect.com/science/article/pii/S0029801817303955?via%3Dihub

Link codice DOI: http://dx.doi.org/10.1016/j.oceaneng.2017.07.025

Citazione bibliografica dell'articolo:

Daniela De Palma, Filippo Arrichiello, Gianfranco Parlangeli, **Giovanni Indiveri**, Underwater localization using single beacon measurements: Observability analysis for a double integrator system, Ocean Engineering, Volume 142, 2017, Pages 650-665,

Underwater localization using single beacon measurements: Observability analysis for a double integrator system

Daniela De Palma[a,*], Filippo Arrichiello[b], Gianfranco Parlangeli[a], Giovanni Indiveri[a]

[a] *Dipartimento di Ingegneria dell'Innovazione, Università del Salento (ISME Node), Via Monteroni, 73100 Lecce, Italy*
[b] *Dipartimento di Ingegneria Elettrica e dell'Informazione, Università degli Studi di Cassino e del Lazio Meridionale (ISME Node), Via G. Di Biasio 43, 03043 Cassino, FR, Italy*

Keywords:
Autonomous Underwater Vehicles
Underwater localization
Range-based localization observability

A B S T R A C T

This paper addresses the observability analysis for the single beacon localization problem of an Autonomous Underwater Vehicle (AUV) modeled as a double integrator where its input is the acceleration in an inertial reference frame and its output (measurement) is its range to a stationary beacon. The nonlinear map between range and position makes the range-based observability problem inherently nonlinear. The observability analysis here proposed addresses two complementary issues: the local weak observability for the nonlinear system, and the global observability for a linear time varying representation of the system derived through a state augmentation method. The proposed methods for observability analysis are discussed in different case studies (e.g. 2D/3D, absence/presence of current, and presence of additional sensors like a Doppler Velocity Logger or a depth gauge). Two different state observers, i.e., an Extended Kalman Filter for the nonlinear system, and a Kalman Filter for the system with augmented state are designed: their performances are analyzed through numerical simulations while validating the derived observability properties.

1. Introduction

The problem of localization of Autonomous Underwater Vehicles (AUVs) during underwater navigation has been widely investigated in recent years. Indeed, during underwater navigation, AUVs cannot rely on Global Navigation Satellite Systems (GNSSs) due to the attenuation of electromagnetic radiation in the water domain and, in the absence of specific positioning systems, they can exclusively relay on dead-reckoning techniques. As the latter approaches integrate noisy and biased measurements from Inertial Measurement Units (IMUs) and velocity sensors, they suffer from numerical drift that makes them usable only for relatively short periods. In these cases, the AUVs are often required to surface in order to acquire a positioning fix from the GNSS.

Commercially available underwater positioning solutions are mainly based on acoustic devices that, through the measurement of the time of flight of acoustic signals, allow to measure the ranges from source to receiving nodes. For example, in Long Base Line (LBL) acoustic localization systems the AUV measures the ranges to a set of transponders placed in fixed and known positions in the sea, and it estimates its position via trilateration algorithms (see e.g. Scherbatyuk, 1995). In Short Base Line (SBL) systems, three or more transducers mounted on a surface vessel request replies from a transponder installed on-board the AUV and, as in the LBL case, the AUV position is estimated via trilateration. In Ultra-short Base Line (USBL) systems, instead, a set of transducers is assembled in a single device installed on board a support ship, and the AUV position is estimated on the base of the phase shifting of the signals arriving at the transducers.

More recently, research efforts focused on positioning systems based on the use of range measurements to a single node with the aim of developing simple, cheap and easy to operate solutions. Such approaches, known in the literature as *single beacon localization*, *single range localization* or *range-only localization*, are based on the fusion of range measurements to the single source with information from AUV's onboard sensors as Inertial Measurement Unit (IMU), Doppler Velocity Logger (DVL) and depth sensors (see for example, Larsen, 2000; Gadre and Stilwell, 2005; Jouffroy and Reger, 2006; Bahr et al., 2009; Webster et al., 2012; Viegas et al., 2012; Crasta et al., 2014, 2015; Bayat et al., 2016). Similar approaches can be considered in the case of multi-vehicle localization where opportunistic range measurements arising from time of flight data associated to acoustic communications devices may be available and can be used for relative localization (see for example, Fallon et al., 2010; Arrichiello et al., 2012; Parlangeli and Indiveri, 2014, 2015; De Palma et al., 2015).

Despite their potential advantages, single beacon localization

* Corresponding author.
E-mail addresses: daniela.depalma@unisalento.it (D. De Palma), f.arrichiello@unicas.it (F. Arrichiello), gianfranco.parlangeli@unisalento.it (G. Parlangeli), giovanni.indiveri@unisalento.it (G. Indiveri).

approaches suffer from observability issues that may affect if, or how well, the system state can be estimated based on the available information (i.e. system model, input and output). Thus, an observability analysis is required to design a state observer and to define under which assumptions the observer may provide proper results. The nonlinear output map between range and position makes the range-based observability problem inherently nonlinear. As a consequence, the observability analysis needs to be addressed in the framework of nonlinear systems, e.g. evaluating the local weak observability properties of the system. This can be done by resorting to the tools of differential algebraic geometry. A major contribution in this area is provided in Hermann and Krener (1977) where the fundamental definitions, ideas and results about local weak observability for nonlinear systems are derived; in particular, the local weak observability properties of a system state can be inferred from the observability rank condition in Hermann and Krener (1977) that yields a *sufficient condition* for it. In Arrichiello et al. (2013), the local weak observability properties for the range-based localization problem of an AUV modeled as a single integrator is addressed, and a metric to analyze how the performance in localization depends on the types of motion imparted to the AUVs is presented.

In order to allow the use of tools for linear systems to analyze the global observability properties, some approaches proposed in the literature rely on *state augmentation* methods. For example, the works in Batista et al. (2011b), Parlangeli et al. (2012), Indiveri and Parlangeli (2013), Indiveri et al. (2016) show that it is possible to represent the system as a linear time varying (LTV) system with augmented state; in this case, the observability of the LTV system with augmented state can be inferred from the analysis of the observability Gramian.

The observability analysis here presented addresses two complementary issues: the local weak observability for the nonlinear system, and the global observability for the LTV system with *augmented state*. Indeed, trajectories that are not globally observable may result locally weakly observable and viceversa, i.e. trajectories that are globally observable are not guaranteed to be locally weakly observable. While addressing the specific issue of range-based observability as outlined above, the paper will also aim at discussing, in more general terms, the relation and dependencies between global and local weak observability for finite dimensional state space systems. With reference to the specific AUV problem at hand, the proposed methods for observability analysis are discussed in different case studies (e.g. 2D/3D, absence/presence of current, presence of additional sensors like Doppler Velocity Logger or depth sensors). Two different state observers, i.e., an Extended Kalman Filter for the nonlinear system and a Kalman Filter for the system with augmented state are designed, and their performances are illustrated throughout numerical simulations and compared referring to the derived observability properties. This work extends our preliminary paper Arrichiello et al. (2015) by providing a more in-depth and formalized analysis of the system observability in the two different cases, and an extended number of case studies and comparison via numerical simulations.

The rest of the paper is organized as follows: Section 2 addresses the system modeling and the range-based observability problem; Section 3 presents a brief review of the key concepts of the observability analysis for nonlinear systems and LTV systems. Section 4 presents the observability analysis referring to local weak observability properties for the nonlinear system and Gramian based observability properties for the LTV system with augmented state. Section 5 addresses the observability properties in different case studies. Section 6 illustrates the effect of additional sensors on the observability properties, while Section 7 reports the results of numerical evaluations using different state observers, i.e. Extended Kalman Filter for the nonlinear system and a Kalman Filter for the system with augmented state. Finally, Section 8 summarizes the conclusions and briefly outlines future works.

2. Problem formulation

With reference to the dynamic model of AUVs, the actuated inputs are forces and torques basically proportional to the vehicles acceleration. As a result, a second order kinematic model is a more realistic approximation of the actual system rather than a first order kinematic model (Hinson et al., 2013). In light of the above consideration, the AUV is modeled as a double integrator where its input is the acceleration in an inertial reference frame and the measured output is proportional to the square of the distance between the AUV and a stationary beacon. Without loss of generality, the beacon is assumed to be located at the origin of the inertial frame. In absence of ocean current, the resulting kinematic vehicle model is given by

$$\dot{\mathbf{p}} = \mathbf{v} \tag{1}$$

$$\dot{\mathbf{v}} = \mathbf{u} \tag{2}$$

$$y = \frac{1}{2}\mathbf{p}^\top\mathbf{p} = \frac{1}{2}\|\mathbf{p}\|^2 \tag{3}$$

where $\mathbf{p} \in \mathbb{R}^n$ denotes the vehicle position, $\mathbf{v} \in \mathbb{R}^n$ the vehicle absolute velocity, $\mathbf{u} \in \mathbb{R}^n$ its acceleration (i.e. the input) and y denotes a measurement proportional to the squared range to the beacon. The dimension n will be either 2 or 3 in the planar and full 3D cases respectively. The resulting state-space model can be expressed as follows:

$$\dot{\mathbf{x}} = \begin{bmatrix} 0_{n\times n} & I_{n\times n} \\ 0_{n\times n} & 0_{n\times n} \end{bmatrix}\mathbf{x} + \begin{bmatrix} 0_{n\times n} \\ I_{n\times n} \end{bmatrix}\mathbf{u} \tag{4}$$

$$y = h(\mathbf{x}) = \frac{1}{2}\mathbf{p}^\top\mathbf{p} = \frac{1}{2}\parallel \mathbf{p} \parallel^2 \tag{5}$$

where $\mathbf{x} = (\mathbf{p}^\top\ \mathbf{v}^\top)^\top \in \mathbb{R}^{2n}$ is the system state, $h(\cdot)$ is a nonlinear output function of the state, $I_{n\times n}$ is an identity matrix of dimension $(n \times n)$ and $0_{n\times n}$ is a matrix of dimension $(n \times n)$ with zero elements.

The state estimation problem for the nonlinear system under investigation is strongly dependent on the input of the system. This motivates the analysis of the state estimation problem for different kinds of trajectories of practical interest.

Problem Statement: Given the linear state equation in (4) and the nonlinear scalar output equation in (5), determine the conditions that allow to estimate the state $\mathbf{x} = (\mathbf{p}^\top\ \mathbf{v}^\top)^\top$, with particular attention to different classes of motions of practical interest, like straight lines, circular or lawn-mowing trajectories. Moreover, design possible state estimators.

3. Observability analysis tools

The observability of the system (4)–(5) can be analyzed resorting to different tools. Given the non linearity of the system (4)–(5), the local weak observability properties will be inferred through the tools of differential algebraic geometry described in Hermann and Krener (1977). On the other hand, resorting to a *state augmentation* method as in Indiveri et al. (2016), the nonlinear system (4)–(5) can be represented in an LTV form making it possible to study observability through the use of well known linear systems' theory methods.

3.1. Observability of nonlinear systems

With reference to a generic nonlinear system

$$\dot{\mathbf{x}}(t) = \mathbf{f}(\mathbf{x}(t), \mathbf{u}(t)), \quad \mathbf{x}(t_0) = \mathbf{x}_0 \tag{6}$$

$$\mathbf{y}(t) = \mathbf{h}(\mathbf{x}(t)) \tag{7}$$

where $\mathbf{x} \in \mathbb{R}^N$, $\mathbf{u} \in \mathbb{R}^Q$, $\mathbf{y} \in \mathbb{R}^M$ and t denote the state, input, output vectors and time respectively, the following definitions are introduced according to the standard system theory (Hermann and Krener, 1977).

Definition 3.1. Given the system defined by Eqs. (6)–(7) and the time interval $[t_0, t_f]$, two initial conditions $\mathbf{x}_0$, $\mathbf{x}_0^*$ are *indistinguishable* in $[t_0, t_f]$ if for all admissible inputs $\mathbf{u}$ the output evolutions of the system are identical.For every $\mathbf{x}_0$, let $\mathcal{I}(\mathbf{x}_0)$ denote the set of all initial conditions that are indistinguishable from $\mathbf{x}_0$ in $[t_0, t_f]$.

Definition 3.2. The system (6)–(7) is said to be *observable at* $\mathbf{x}_0$ in $[t_0, t_f]$ if $\mathcal{I}(\mathbf{x}_0) = \{\mathbf{x}_0\}$, and it is said to be *observable* (in all the states) if $\mathcal{I}(\mathbf{x}) = \{\mathbf{x}\}$ for every state $\mathbf{x}$ of the state space.As widely highlighted in Hermann and Krener (1977), note that the observability property is a global concept in the sense that it refers to the injectivity of the output evolution operator with respect to the initial conditions; it might be necessary to travel a considerable distance or for a long time for two states to be distinguishable. Therefore, the *local weak observability* property is introduced; intuitively, a system is *locally weakly observable* if one can instantaneously distinguish each state from its neighbours.

Definition 3.3. The system (6)–(7) is said to be *locally weakly observable at* $\mathbf{x}_0$ if there exists an open neighborhoud U of $\mathbf{x}_0$ such that for every open neighborhoud V of $\mathbf{x}_0$ contained in U, $\mathcal{I}(\mathbf{x}_0) = \{\mathbf{x}_0\}$, and it is said to be *locally weakly observable* if it is so at every state $\mathbf{x}$ of the state space.

For linear systems, these properties are equivalent. The advantage of local weak observability is that it lends itself to a simple algebraic test. In particular, the local weak observability properties of a system can be inferred from the observability rank condition in Hermann and Krener (1977) (Theorem 3.1, page 733) that yields a *sufficient condition* for it.

Before enunciating the latter condition, recall the definition of Lie derivatives of the scalar output, h_j, for the system in Eqs. (6)–(7) as:

$$\begin{aligned}
&\mathcal{L}_f^0 h_j = h_j \\
&\mathcal{L}_f^1 h_j = \nabla h_j \cdot \mathbf{f} = \sum_{i=1}^{N} \frac{\partial h_j}{\partial x_i} \cdot f_i \\
&\mathcal{L}_f^2 h_j = \nabla[\mathcal{L}_f^1 h_j] \cdot \mathbf{f} \\
&\cdots \\
&\mathcal{L}_f^l h_j = \nabla[\mathcal{L}_f^{l-1} h_j] \cdot \mathbf{f}
\end{aligned} \tag{8}$$

with ∇ denoting the gradient operator and $\mathcal{L}_f^a h_j$ being the set of the a-order Lie derivatives for any $j \in \{1, \ldots, M\}$.

Theorem 3.4. *Considering the system (6)–(7), if there exists an input,* $\mathbf{u}$*, such that the matrix*

$$O := \begin{bmatrix} \nabla \mathcal{L}_f^0 h_j \\ \nabla \mathcal{L}_f^1 h_j \\ \vdots \\ \nabla \mathcal{L}_f^k h_j \end{bmatrix} \tag{9}$$

computed at $\mathbf{x}_1$ *has rank* N *for some index* $k \in \mathbb{N}$*, then the system (6)–(7) is locally weakly* observable *at* $\mathbf{x}_1$.It is worth remarking that the latter is a *sufficient condition*, thus, in case it is not satisfied, one cannot infer that the system is not locally weakly observable.

3.2. Observability of linear time varying systems

With reference to a generic LTV system

$$\dot{\mathbf{x}}(t) = A(t)\mathbf{x}(t) + B(t)\mathbf{u}(t), \quad \mathbf{x}(t_0) = \mathbf{x}_0 \tag{10}$$

$$\mathbf{y}(t) = C(t)\mathbf{x}(t) \tag{11}$$

where $\mathbf{x} \in \mathbb{R}^N$, $\mathbf{u} \in \mathbb{R}^Q$, $\mathbf{y} \in \mathbb{R}^M$ and t are the state, input, output vectors and time respectively, and $A(t)$, $B(t)$, $C(t)$ are matrices with appropriate dimensions, the following definitions are introduced according to the standard linear systems theory (see e.g. Kalman, 1960; Rugh, 1996).

Definition 3.5. An initial state $\mathbf{x}_0$ of the LTV system (10)–(11) is *observable on* $[t_0, t_f]$ if it is uniquely determined by the corresponding output $\boldsymbol{y}(t)$ for $t \in [t_0, t_f]$. If this is true for every initial state $\mathbf{x}_0$, the system is *completely observable on* $[t_0, t_f]$; if this is true for every t_0, the system is *completely observable*.

Definition 3.6. The observability Gramian associated with the pair $(A(t), C(t))$ denoted as $G(t_0, t_f)$, is given by

$$G(t_0, t_f) = \int_{t_0}^{t_f} \Phi^\top(t, t_0) C^\top(t) C(t) \Phi(t, t_0) dt,$$

where $\Phi(t, t_0)$ is the transition matrix associated with $A(t)$.

The observability Gramian is a useful observability analysis tool for linear time varying systems, indeed the following theorem (Rugh, 1996, Theorem 9.8, page 148) and definition (Kalman, 1960) hold.

Theorem 3.7. *The LTV system (10)–(11) is observable on* $[t_0, t_f]$ *if and only if* $G(t_0, t_f)$ *is invertible.*

Definition 3.8. The LTV system (10)–(11) is *uniformly completely observable* if there exist positive constants δ, α_1 and α_2 such that

$$\alpha_1 I \leq G(t, t + \delta) \leq \alpha_2 I \tag{12}$$

for all $t \geq t_0$.

4. Observability analysis for the range-based localization problem and filter design

4.1. Local weak observability

The analysis of local weak observability of the nonlinear system (4)–(5) can be approached as described in Section 3.1. The observability matrix O in (9) for the system under investigation takes the form:

$$O = \begin{bmatrix} \mathbf{p}^\top & 0_{1\times n} \\ \mathbf{v}^\top & \mathbf{p}^\top \\ \mathbf{u}^\top & 2\mathbf{v}^\top \\ 0_{1\times n} & 3\mathbf{u}^\top \\ 0_{1\times n} & 0_{1\times n} \\ \vdots & \vdots \end{bmatrix}. \tag{13}$$

Local weak observability condition: From Theorem 3.4 for nonlinear systems, it follows that if there exists an $\mathbf{u}$ such that the matrix O in (13) computed in $\mathbf{x}_1$ has full column rank, then the system (4)–(5) is locally weakly observable at $\mathbf{x}_1$. It is worth noting that the local weak observability condition of a state is verified if there exists an input that verifies the observability matrix rank condition, however the latter condition must not be verified for all the possible inputs. This means that, even if the system may result locally weakly observable at a given state $\mathbf{x}_1$, there may exist inputs for which $\mathcal{I}(\mathbf{x}_1) \neq \{\mathbf{x}_1\}$. Indeed, in other studies as Bayat et al. (2016) the observability concept is redefined with respect to a reduced class of inputs rather than for all inputs that are physically admissible. Our aim is thus to identify, on the base of the rank of the matrix O, if some inputs, in a given state, ensure $\mathcal{I}(\mathbf{x}_1) = \{\mathbf{x}_1\}$.

Moreover, with a slight abuse of notation, in the following the states generated by inputs granting full column rank of the observability matrix (13) at all times are denoted as "*locally weakly observable along the trajectory*".

In the following, the performance of an Extended Kalman Filter (EKF) is evaluated as a possible state observer in relation with the local weak observability properties of specific trajectories of the system. It is worth noting that both the previously defined observability properties and the EKF convergence properties hold locally; thus, even when the system is locally weakly observable along an assigned trajectory, if the initial state estimate of the EKF is not sufficiently close to the true initial state, there is no guarantee that the estimation error converges to zero.

4.2. Global observability

The observability analysis of system (4)–(5) can also be studied as in Indiveri et al. (2016) where the range-based observability problem of a first order kinematic model is addressed. In Indiveri et al. (2016), a *state augmentation* method is used to re-elaborate the nonlinear system equations so that the observability problem can be approached with the tools used for LTV systems. To the purpose, consider the integral of Eqs. (1)–(2)

$$\begin{aligned}\mathbf{p}(t) &= \mathbf{p}_0 + \mathbf{v}_0(t-t_0) + \int_{t_0}^{t}\int_{t_0}^{\tau_1}\mathbf{u}(\tau_2)d\tau_2 d\tau_1 \\ &= \mathbf{p}_0 + \mathbf{v}_0(t-t_0) + \mathbf{d}(t,t_0)\end{aligned} \tag{14}$$

having defined the displacement $\mathbf{d}(t, t_0) \in \mathbb{R}^n$ as

$$\mathbf{d}(t,t_0) := \int_{t_0}^{t}\int_{t_0}^{\tau_1}\mathbf{u}(\tau_2)d\tau_2 d\tau_1 \tag{15}$$

and

$$\mathbf{p}_0 := \mathbf{p}(t)|_{t=t_0}. \tag{16}$$

Eq. (14) can be put in the form

$$\begin{aligned}&[\mathbf{p}(t)-\mathbf{d}(t,t_0)]^{\top}[\mathbf{p}(t)-\mathbf{d}(t,t_0)]= \\ &=[\mathbf{p}_0 + \mathbf{v}_0(t-t_0)]^{\top}[\mathbf{p}_0 + \mathbf{v}_0(t-t_0)]\end{aligned} \tag{17}$$

implying

$$\begin{aligned}&\tfrac{1}{2}\|\mathbf{p}(t)\|^2-\tfrac{1}{2}\|\mathbf{p}_0\|^2 + \tfrac{1}{2}\|\mathbf{d}(t,t_0)\|^2= \\ &=\mathbf{d}(t,t_0)^{\top}\mathbf{p}(t) + \mathbf{p}_0^{\top}\mathbf{v}_0(t-t_0) + \tfrac{1}{2}\|\mathbf{v}_0\|^2(t-t_0)^2.\end{aligned} \tag{18}$$

Note that the left hand side of (18) is made of all known terms and it can be used as a new output map

$$\begin{aligned}\bar{y}(t) &= \tfrac{1}{2}\|\mathbf{p}(t)\|^2-\tfrac{1}{2}\|\mathbf{p}_0\|^2 + \tfrac{1}{2}\|\mathbf{d}(t,t_0)\|^2 \\ &= y(t)-y_0 + \tfrac{1}{2}\|\mathbf{d}(t,t_0)\|^2,\end{aligned} \tag{19}$$

moreover, the right hand side of (18) can be expressed as an LTV term in the new state variable $\mathbf{z} \in \mathbb{R}^{2n+2}$

$$\mathbf{z} = (\mathbf{p}^{\top}, \mathbf{v}^{\top}, \mathbf{p}_0^{\top}\mathbf{v}_0, \|\mathbf{v}_0\|^2)^{\top}, \tag{20}$$

i.e.

$$\bar{y}(t) = C(t)\mathbf{z} = \begin{pmatrix}\mathbf{d}^{\top}(t,t_0) & \mathbf{0}_{1\times n} & (t-t_0) & \frac{1}{2}(t-t_0)^2\end{pmatrix}\mathbf{z}. \tag{21}$$

Given the definition of $\mathbf{z}$ in (20) and the model (1-2), its dynamic equation is linear time invariant (LTI):

$$\dot{\mathbf{z}} = A\mathbf{z} + B\mathbf{u} \tag{22}$$

namely

$$\dot{\mathbf{z}} = \frac{d}{dt}\begin{pmatrix}\mathbf{p}\\ \mathbf{v}\\ \mathbf{x}_0^{\top}\mathbf{v}_0\\ \|\mathbf{v}_0\|^2\end{pmatrix} = \begin{bmatrix}0_{n\times n} & I_{n\times n} & 0_{n\times 1} & 0_{n\times 1}\\ 0_{n\times n} & 0_{n\times n} & 0_{n\times 1} & 0_{n\times 1}\\ 0_{1\times n} & 0_{1\times n} & 0 & 0\\ 0_{1\times n} & 0_{1\times n} & 0 & 0\end{bmatrix}\begin{pmatrix}\mathbf{p}\\ \mathbf{v}\\ \mathbf{x}_0^{\top}\mathbf{v}_0\\ \|\mathbf{v}_0\|^2\end{pmatrix} + \begin{bmatrix}0_{n\times n}\\ I_{n\times n}\\ 0_{1\times n}\\ 0_{1\times n}\end{bmatrix}\mathbf{u}. \tag{23}$$

The range-based localization problem of estimating the position $\mathbf{p}$ and the velocity $\mathbf{v}$ from a measurement proportional to $\|\mathbf{p}\|^2$ in Eqs. (4)–(5) is hence reduced to a state estimation problem on a LTI state equation (22)–(23) with an LTV output map (21), namely

$$\begin{cases}\dot{\mathbf{z}} = A\,\mathbf{z} + B\,\mathbf{u}\\ \bar{y}(t) = C(t)\,\mathbf{z}.\end{cases} \tag{24}$$

Therefore, the global observability properties of the original nonlinear system (4)–(5) can be inferred using Gramian based tools for LTV systems applied to the augmented system (24). Note that the output map $C(t)$ in (21) is a function of the input term $\mathbf{u}(t)$, hence the observability properties will depend on the acceleration input $\mathbf{u}(t)$. Let us consider the observability Gramian of the system (24) defined as

$$G(t,t_0) = \int_{t_0}^{t} e^{A^{\top}(\tau-t_0)}C^{\top}(\tau)C(\tau)e^{A(\tau-t_0)}d\tau \tag{25}$$

Given the structure of the matrix A in (23), note that $A^2 = 0_{(2n+2)\times(2n+2)}$ and the exponential matrix $e^{A(\tau-t_0)}$ is simply

$$e^{A(\tau-t_0)} = I_{(2n+2)\times(2n+2)} + A(\tau-t_0) \tag{26}$$

such that

$$e^{A^{\top}(\tau-t_0)}C^{\top}(\tau)C(\tau)e^{A(\tau-t_0)} = \begin{bmatrix}\mathbf{d}\mathbf{d}^{\top} & (\tau-t_0)\mathbf{d}\mathbf{d}^{\top} & (\tau-t_0)\mathbf{d} & \frac{(\tau-t_0)^2\mathbf{d}}{2}\\ (\tau-t_0)\mathbf{d}\mathbf{d}^{\top} & (\tau-t_0)^2\mathbf{d}\mathbf{d}^{\top} & (\tau-t_0)^2\mathbf{d} & \frac{(\tau-t_0)^3\mathbf{d}}{2}\\ (\tau-t_0)\mathbf{d}^{\top} & (\tau-t_0)^2\mathbf{d}^{\top} & (\tau-t_0)^2 & \frac{(\tau-t_0)^3}{2}\\ \frac{(\tau-t_0)^2\mathbf{d}^{\top}}{2} & \frac{(\tau-t_0)^3\mathbf{d}^{\top}}{2} & \frac{(\tau-t_0)^3}{2} & \frac{(\tau-t_0)^4}{4}\end{bmatrix} \tag{27}$$

where the dependence of $\mathbf{d}$ from (τ, t_0) has been omitted for the sake of notation compactness.

Global observability condition: From the standard results for LTV systems (Theorem 3.7) it follows that the system (24) is observable on the time interval $[t_0, t]$ if and only if the acceleration input $\mathbf{u}(t)$ guarantees that, for some $t_a \in [t_0, t]$, the observability Gramian $G(t_0, t_a)$ in Eqs. (25) and (27) has full rank. This is a necessary and sufficient condition for the observability of the LTV system (24). Finally, the observability of the LTV model in (24) is a sufficient, but not necessary, condition to grant the observability of the original model in (4)–(5). For further details about this observability condition the reader is referred to Indiveri et al. (2016).

If this condition is satisfied, the nonlinear system is globally observable and a standard Kalman filter can be designed on the LTV system for global state estimation. Uniform complete observability of the LTV system is required to ensure that the Kalman filter is asymptotically stable. It is worth highlighting that if the input $\mathbf{u}$ of the LTV system is bounded, then it can be proven that the observability implies the uniform complete observability of the system (Batista et al., 2011a; Silverman and Anderson, 1968; Jazwinski, 2007).

With reference to the Gramian in (25) and (27), note that its entries have different time scaling behaviors. By example, in the last column of (27) there is a dependency on the fourth power of time as opposed to the first column where there is only a dependency on the second power of time. This can lead to numerical ill conditioning issues over longer time intervals affecting the numerical assessment of the rank of $G(t, t_0)$ in (25). Nevertheless, this is not a problem in practice as $G(t, t_0)$ can always be decomposed as a sum

$$G(t,t_0) = \sum_{i=0}^{N-1} G(t_{i+1}, t_i) \quad : \quad t_0 \le t_1 \le t_2 \le \ldots \le t_{N=t}$$

where each term in the sum is a positive (semi) definite symmetric matrix. If any term of the sum should be positive definite, then the whole sum would be positive definite, i.e. full rank. It follows that in order to verify the full rankness of $G(t, t_0)$ one can evaluate the full rankness of the terms in the sum: being these terms computed on an arbitrarily small time interval, their condition number cannot diverge due to the difference between t_{i+1} and t_i.

4.3. Remark: presence of unknown ocean current

The described approach can be extended to the case where the vehicle is subject to a constant and unknown ocean current. The resulting kinematic vehicle model is given by

$$\dot{\mathbf{p}} = \mathbf{v} + \mathbf{v}_f \tag{28}$$

$$\dot{\mathbf{v}}_f = \mathbf{0} \tag{29}$$

$$\dot{\mathbf{v}} = \mathbf{u} \tag{30}$$

$$y = \frac{1}{2} \| \mathbf{p} \|^2 \tag{31}$$

where $\mathbf{v} \in \mathbb{R}^n$ denotes the vehicle velocity with respect to the fluid and $\mathbf{v}_f \in \mathbb{R}^n$ the ocean current assumed constant in the inertial frame. Interestingly, with the variable transformation $\boldsymbol{\nu} = \mathbf{v} + \mathbf{v}_f$, the system (28)–(31) becomes

$$\dot{\mathbf{p}} = \boldsymbol{\nu} \tag{32}$$

$$\dot{\boldsymbol{\nu}} = \mathbf{u} \tag{33}$$

$$y = \frac{1}{2} \| \mathbf{p} \|^2 \tag{34}$$

that, clearly, resembles the system in (1)–(2). This allows to gather that the system in presence of ocean current (28)–(31) is not observable; indeed, the observable states are the position $\mathbf{p}$ and the cumulative velocity $\boldsymbol{\nu}$ only, while the vehicle velocity with respect to the fluid $\mathbf{v}$ and the ocean current $\mathbf{v}_f$ cannot be distinguished the one from the other. This result is confirmed by the global observability analysis. The details of these analysis are omitted for the sake of brevity. In short, the observability Gramian associated to the LTV representation of the nonlinear system (28)–(31) (obtained through the *state augmentation* method) is rank deficient and leads to a violation of the observability condition. It can also be noted that the matrix O in (9) derived for the system under investigation is rank deficient for all $\mathbf{x} \in \mathbb{R}^{2n}$ and for any choice of the input $\mathbf{u}$, therefore observability rank condition is not satisfied.

5. Case studies

5.1. 2D model

Let us consider the 2D version ($n = 2$) of the system (4)–(5). The matrix O for the analysis of the local weak observability has the following form:

$$O = \begin{bmatrix} p_x & p_y & 0 & 0 \\ v_x & v_y & p_x & p_y \\ u_x & u_y & 2v_x & 2v_y \\ 0 & 0 & 3u_x & 3u_y \end{bmatrix} \tag{35}$$

with $\mathbf{p} = (p_x, p_y)^\top$, $\mathbf{v} = (v_x, v_y)^\top$ and $\mathbf{u} = (u_x, u_y)^\top$ denoting the coordinates of the position, velocity and input of the vehicle along the x, y inertial axes, respectively. In such a case, the state vector $\mathbf{x}$ has dimension $2n = 4$, hence the local weak observability condition at a generic state $\mathbf{x}_1$ is satisfied if there exists an input $\mathbf{u}$ such that the matrix O has rank 4. Note that the observability of the system at $\mathbf{x}_1$ does not imply that every input makes the state distinguishable from close states. Our analysis is focused on inputs that generate classes of motion of practical interest, like straight line, circular or lawn-mowing trajectories. It is worth noting that a null input, i.e. $\mathbf{u} = (u_x, u_y)^\top = (0, 0)^\top$ will cause a rank deficiency; hence a null acceleration (constant velocity) will not allow to infer the local weak observability properties from the observability rank condition.

Let us analyze the local weak observability condition along straight line trajectories described by the equation $p_y = m\, p_x + q$, where m denotes the slope and q denotes the y intercept. The determinant of the observability matrix along such a class of motion is

$$\det(O) = -3u_x^2 q^2 \neq 0 \Leftrightarrow \begin{cases} u_x \neq 0 \\ q \neq 0 \end{cases}. \tag{36}$$

As a result, if the input signal and the y intercept are not null, the matrix O is full rank. This allows to gather that straight line trajectories performed at non uniform velocity and not passing through the origin where the beacon is located are locally weakly observable. Whereas, the observability matrix along radial trajectories ($q = 0$), i.e. a line passing through the beacon, has rank 2; hence, the local weak observability properties can not be inferred from the observability rank condition.

A similar analysis can be undertaken for circular trajectories centered on the beacon, i.e. described by the following equations

$$\begin{pmatrix} p_x \\ p_y \end{pmatrix} = \begin{pmatrix} \rho \cos(\omega t) \\ \rho \sin(\omega t) \end{pmatrix} \tag{37}$$

where ρ denotes the radius of the circumference and ω the angular velocity along the circumference. It can be shown, by direct calculation, that the determinant of the matrix O in any state along circular trajectories is not null:

$$\det(O) = 6\,\omega^4 \rho^4 \neq 0 \quad \forall\ t \in \mathbb{R}, \quad \omega \neq 0, \quad \rho \neq 0$$

therefore the matrix O has full rank and the local weak observability condition is satisfied. This should not surprise, in fact, as shown in Arrichiello et al. (2013) and Hinson et al. (2013), with reference to the first order kinematic model, the circular trajectory is optimal from an observability point of view. If the trajectory results locally weakly observable, an observer can be designed to estimate the state (position and velocity) of the vehicle and the estimated state will converge to the true one as long as the initial state estimate is sufficiently close to the true one. Given the non linearity of the output equation, a possible observer is an Extended Kalman Filter.

As opposed to the use of the local weak observability condition that captures the instantaneous motion, the global observability analysis derived from the observability Gramian in (25)–(27) takes into account the whole trajectory. The equations of the observability Gramian allow to conclude that if $\mathbf{d}(t, t_0) = \mathbf{0}$, the rank observability condition is not satisfied. This occurs, for example, when the input $\mathbf{u}$ is null (i.e. trajectory with constant velocity). Further results can be derived through numerical simulations as reported in the following section. In particular it can be verified, by direct calculation, that straight line motions do not satisfy the full rank condition for $G(t, t_0)$, so global observability properties can not be inferred. Whereas circular trajectories ensure the full rank of the observability Gramian. Interestingly, by concatenation of circular and straight line motions in a lawn-mowing trajectory, it is possible to achieve an observable system. Indeed, the LTV system theory ensures that if a system is observable in the interval $[t_0, t_a]$, it is also observable in the interval $[t_0, t]$ with $t > t_a$.

5.2. 3D model

Let us consider the 3D version ($n = 3$) of the system (4)–(5). The matrix O for the analysis of the local weak observability has the following form:

$$O = \begin{bmatrix} p_x & p_y & p_z & 0 & 0 & 0 \\ v_x & v_y & v_z & p_x & p_y & p_z \\ u_x & u_y & u_z & 2v_x & 2v_y & 2v_z \\ 0 & 0 & 0 & 3u_x & 3u_y & 3u_z \end{bmatrix} \tag{38}$$

with $\mathbf{p} = (p_x, p_y, p_z)^\top$, $\mathbf{v} = (v_x, v_y, v_z)^\top$ and $\mathbf{u} = (u_x, u_y, u_z)^\top$ denoting the coordinates of the position, velocity and input of the vehicle along the x, y, z inertial axes, respectively. In such a case, the state vector $\mathbf{x}$ has dimension $2n = 6$, so for the local weak observability condition the rank of O should be equal to 6. It is worth highlighting that since the matrix O in (38) has only 4 rows different from zero, the local weak observability condition can never be satisfied. It is important to note that the loss of the observability rank condition at one point does not necessarily imply local unobservability. With reference to the global observability analysis, let us consider the 3D version of the observability Gramian in (25)–(27). Like for the 2D model, trajectories with constant velocity ($\mathbf{u} = \mathbf{0}$) does not satisfy the global observability condition. In general, planar trajectories with $u_z = 0$ (hence not sufficiently rich on the z axis) does not satisfy the observability condition. In such a case, the z component of the displacement

Table 1
Observability along different trajectories for the range only localization according to the local weak observability (LWO) condition and global observability (O) condition for the proper LTV system with augmented state.

	Motion	LWO	O
2D	Straight (radial)	NO	NO
	Straight (not radial)	YES	NO
	Circular	YES	YES
	Circular + Straight (radial)	YES	YES
	Circular + Straight (not radial)	YES	YES
3D	Straight (radial and not radial)	NO	NO
	Circular	NO	NO
	Circular in (x, y) and suff. exciting along z axis	NO	YES
	Circular in (x, y) and suff. exciting along z axis + Straight	NO	YES
	2D/3D with ocean currents	NO	NO

$\mathbf{d}(t, t_0)$ is zero leading to a loss of the observability rank condition. Indeed, in order to satisfy the observability condition, the trajectories should be sufficiently exciting over all axes x, y and z. The results of the observability analysis are summarized in Table 1.

6. Effects of additional sensors

The observability analyses described so far are related to the presence of the sole range measurements. If other measurements are available, such as depth or velocity measurements from a depth sensor or Doppler Velocity Logger (DVL) respectively, the observability properties can be improved.

In presence of a depth sensor, the vertical components of motion can be measured directly; therefore the 3D localization problem will reduce to the 2D localization problem previously discussed preserving the observability properties.

With regards to first order kinematic models of AUV, the observability problem considering both range and depth measurements has been addressed for example in Gadre and Stilwell (2004) and Arrichiello et al. (2013). In Gadre and Stilwell (2004), due to the presence of depth sensors, the authors study the observability for underwater vehicles evolving in 2D. The nonlinear system is linearized about nominal trajectories and standard LTV observability tools are used to analyze the observability properties of the resulting linear model. This leads to local observability conditions. In Arrichiello et al. (2013), the local weak observability properties are addressed, and a metric to analyze how the performance in localization depends on the types of motion imparted to the AUVs is presented. The main contribution with respect to this existing literature is relative to the study of the observability for a double integrator system considering both the local weak observability properties and the global ones.

The observability of range based navigation for first order kinematic models of AUV considering range, depth and velocity measurements has been addressed in Larsen (2000), Jouffroy and Reger (2006), Fallon et al. (2010), Arrichiello et al. (2012), Webster et al. (2012). Larsen (2000) developed an approach called Synthetic LBL, which used measurements from a single acoustic transponder to constrain the error growth of a high performance Inertial Navigation System (INS). In Jouffroy and Reger (2006) the authors propose an algebraic estimator for the estimation of an underwater vehicle using a single acoustic transponder. Fallon et al. (2010) describes the experimental implementation of cooperative localization of multiple AUVs, using a single surface vehicle to aid the navigation of submerged vehicles by providing georeferenced range measurements. A study of the local weak observability of the system is presented and the performance of three estimators have been compared: Particle Filtering (PF), Nonlinear Least Squares optimizer (NLS), and EKF. In Arrichiello et al. (2012) the authors characterizes the localization performance of an Autonomous Underwater Vehicle that takes advantage of relative measurements of range to drifters or surface vessels present in the area. An EKF is performed for an AUV localization. Webster et al. (2012) reports simulation and deep-water sea trials evaluating single beacon navigation based on range measurements between the vehicle and a ship. The single beacon navigation is implemented with a centralized EKF which has access to both ship and vehicle sensor data.

With respect to these works, in this section the local weak and global observability analysis in the 3D case for a double integrator system considering only range and DVL readings (without using depth measurements) is addressed. In presence of a DVL the output equation of the model in (3) becomes

$$\mathbf{y} = \begin{bmatrix} y_1 \\ \mathbf{y}_2 \end{bmatrix} = \begin{bmatrix} \frac{1}{2}\mathbf{p}^\top \mathbf{p} \\ \mathbf{v} \end{bmatrix}, \tag{39}$$

and the observability matrix O for the analysis of the local weak observability takes the form in (40).

$$O = \begin{bmatrix} \mathbf{p}^\top & 0_{1\times n} \\ \mathbf{v}^\top & \mathbf{p}^\top \\ \mathbf{u}^\top & 2\mathbf{v}^\top \\ 0_{1\times n} & 3\mathbf{u}^\top \\ 0_{1\times n} & 0_{1\times n} \\ \vdots & \vdots \\ 0_{n\times n} & I_{n\times n} \\ 0_{n\times n} & 0_{n\times n} \\ \vdots & \vdots \end{bmatrix}. \tag{40}$$

On the other side, with reference to the global observability analysis, the output equation of the augmented LTV system (24) can be rewritten as:

$$\mathbf{y} = \begin{bmatrix} \bar{y} \\ \mathbf{y}_2 \end{bmatrix} = \begin{bmatrix} \mathbf{d}^\top(t, to) & 0_{1\times n} & (t - t_0) & \frac{1}{2}(t - t_0)^2 \\ 0_{n\times n} & I_{n\times n} & 0_{n\times 1} & 0_{n\times 1} \end{bmatrix} \mathbf{z} = C\mathbf{z}, \tag{41}$$

and the observability Gramian becomes:

$$G(t, t_0) = \int_{t_0}^{t} e^{A^\top(\tau - t_0)} C^\top(\tau) C(\tau) e^{A(\tau - t_0)} d\tau$$

$$= \int_{t_0}^{t} \begin{bmatrix} \mathbf{d}\mathbf{d}^\top & (\tau - t_0)\mathbf{d}\mathbf{d}^\top & (\tau - t_0)\mathbf{d} & \frac{(\tau - t_0)^2 \mathbf{d}}{2} \\ (\tau - t_0)\mathbf{d}\mathbf{d}^\top & (\tau - t_0)^2 \mathbf{d}\mathbf{d}^\top + I_{n\times n} & (\tau - t_0)^2 \mathbf{d} & \frac{(\tau - t_0)^3 \mathbf{d}}{2} \\ (\tau - t_0)\mathbf{d}^\top & (\tau - t_0)^2 \mathbf{d}^\top & (\tau - t_0)^2 & \frac{(\tau - t_0)^3}{2} \\ \frac{(\tau - t_0)^2 \mathbf{d}^\top}{2} & \frac{(\tau - t_0)^3 \mathbf{d}^\top}{2} & \frac{(\tau - t_0)^3}{2} & \frac{(\tau - t_0)^4}{4} \end{bmatrix} d\tau. \tag{42}$$

The local weak and global observability properties of the range-based localization problem in presence of DVL measurements will be deeper investigated in the following. Particular emphasis will be dedicated to those classes of trajectories that do not satisfy the observability conditions with range-only measurements.

6.1. 2D model in presence of Doppler Velocity Logger

The local weak observability matrix O for the 2D version of the model (4-39) is given by

$$O = \begin{bmatrix} p_x & p_y & 0 & 0 \\ v_x & v_y & p_x & p_y \\ u_x & u_y & 2v_x & 2v_y \\ 0 & 0 & 3u_x & 3u_y \\ 0 & 0 & 1 & 0 \\ 0 & 0 & 0 & 1 \end{bmatrix}. \tag{43}$$

A first observability analysis is focused on radial trajectories (i.e. linear ones passing through the beacon position). With respect to the case with range only measurements, the presence of DVL allows to

Table 2
Observability along different trajectories with range and DVL measurements according to the local weak observability (LWO) condition and global observability (O) condition for the proper LTV system with augmented state.

		range		range + DVL	
	Motion	**LWO**	**O**	**LWO**	**O**
2D	Straight (radial)	NO	NO	NO	NO
	Straight (not radial)	YES	NO	YES	NO
	Circular	YES	YES	YES	YES
	Circular + Straight (radial)	NO	YES	NO	YES
	Circular + Straight (not radial)	YES	YES	YES	YES
3D	Straight (radial and not radial)	NO	NO	NO	NO
	Circular (in the plane of the beacon)	NO	NO	NO	NO
	Circular (out of the plane of the beacon)	NO	NO	YES	NO
	Circular in (x, y) and suff. excit. along z axis	NO	YES	YES	YES
	Circular in (x, y) and suff. excit. along z axis + Straight	NO	YES	NO	YES

Table 3
Observability with range and DVL measurements in presence of ocean currents according to the local weak observability (LWO) condition and global observability (O) condition for the proper LTV system with augmented state.

		range + DVL (bottom lock)		range + DVL (water profiling)	
	Motion	**LWO**	**O**	**LWO**	**O**
2D	Straight and circular	NO	NO	YES	NO
3D	Straight and circular	NO	NO	NO	NO

increase the rank of the observability matrix from 2 to 3, but it is not yet enough to ensure the local weak observability condition. Also direct calculations of the observability Gramian in (42) for straight trajectories (both radial and not radial) show that its rank increases from 4 to 5. Hence it is still rank deficiency preventing the observability of the LTV augmented system.

6.2. 3D model in presence of DVL

The local weak observability matrix O for the 3D version of the model (4-39) is given by

$$O = \begin{bmatrix} p_x & p_y & p_z & 0 & 0 & 0 \\ v_x & v_y & v_z & p_x & p_y & p_z \\ u_x & u_y & u_z & 2v_x & 2v_y & 2v_z \\ 0 & 0 & 0 & 3u_x & 3u_y & 3u_z \\ 0 & 0 & 0 & 1 & 0 & 0 \\ 0 & 0 & 0 & 0 & 1 & 0 \\ 0 & 0 & 0 & 0 & 0 & 1 \end{bmatrix}. \tag{44}$$

Contrary to the scenario with range only measurements where the local weak observability condition can never be satisfied due to the very structure of the observability matrix, in such a case the matrix O has 7 non null rows. Hence, the local weak observability condition can be satisfied if its rank is equal to $2n = 6$. Nevertheless inputs generating straight line trajectories do not allow to satisfy the local weak observability condition. Indeed, the matrix O along straight line trajectories in $\mathbb{R}^3$ passing through a generic point (x_0, y_0, z_0) and parallel to a generic vector $(b_x, b_y, b_z) \neq \mathbf{0}$ has the following form:

$$O = \begin{bmatrix} p_x & y_0 + \frac{b_y(p_x - x_0)}{b_x} & z_0 + \frac{b_z(p_x - x_0)}{b_x} & 0 & 0 & 0 \\ v_x & \frac{b_y}{b_x} v_x & \frac{b_z}{b_x} v_x & p_x & y_0 + \frac{b_y(p_x - x_0)}{b_x} & z_0 + \frac{b_z(p_x - x_0)}{b_x} \\ u_x & \frac{b_y}{b_x} u_x & \frac{b_z}{b_x} u_x & 2v_x & 2\frac{b_y}{b_x} v_x & 2\frac{b_z}{b_x} v_x \\ 0 & 0 & 0 & 3u_x & 3\frac{b_y}{b_x} u_x & 3\frac{b_z}{b_x} u_x \\ 0 & 0 & 0 & 1 & 0 & 0 \\ 0 & 0 & 0 & 0 & 1 & 0 \\ 0 & 0 & 0 & 0 & 0 & 1 \end{bmatrix} \tag{45}$$

The rank of matrix O in (45) is 4 along radial trajectories and 5 along not radial straight trajectories, i.e. it is rank deficient (rank $(O) \neq 2n$) in both cases. With regards to the observability Gramian in (42), direct calculations for straight trajectories (both radial and not radial) show that its rank increases from 6 to 7 (from 4 to 6 for radial ones). Again, the Gramian observability condition is not satisfied.

Interestingly, in case of circular motions the presence of DVL measurements can be enough to ensure the local weak observability. Let us consider the circular motion described by the following equations

$$\begin{pmatrix} p_x \\ p_y \\ p_z \end{pmatrix} = \begin{pmatrix} \rho \cos(\omega t) \\ \rho \sin(\omega t) \\ q_z \end{pmatrix} \tag{46}$$

where ρ denotes the radius of the circumference in (x, y) plane, ω the angular velocity along the circumference, and q_z a constant depth along the z axis. It can be shown, by direct calculation, that if $q_z \neq 0$, the local weak observability matrix O along the considered trajectory is full

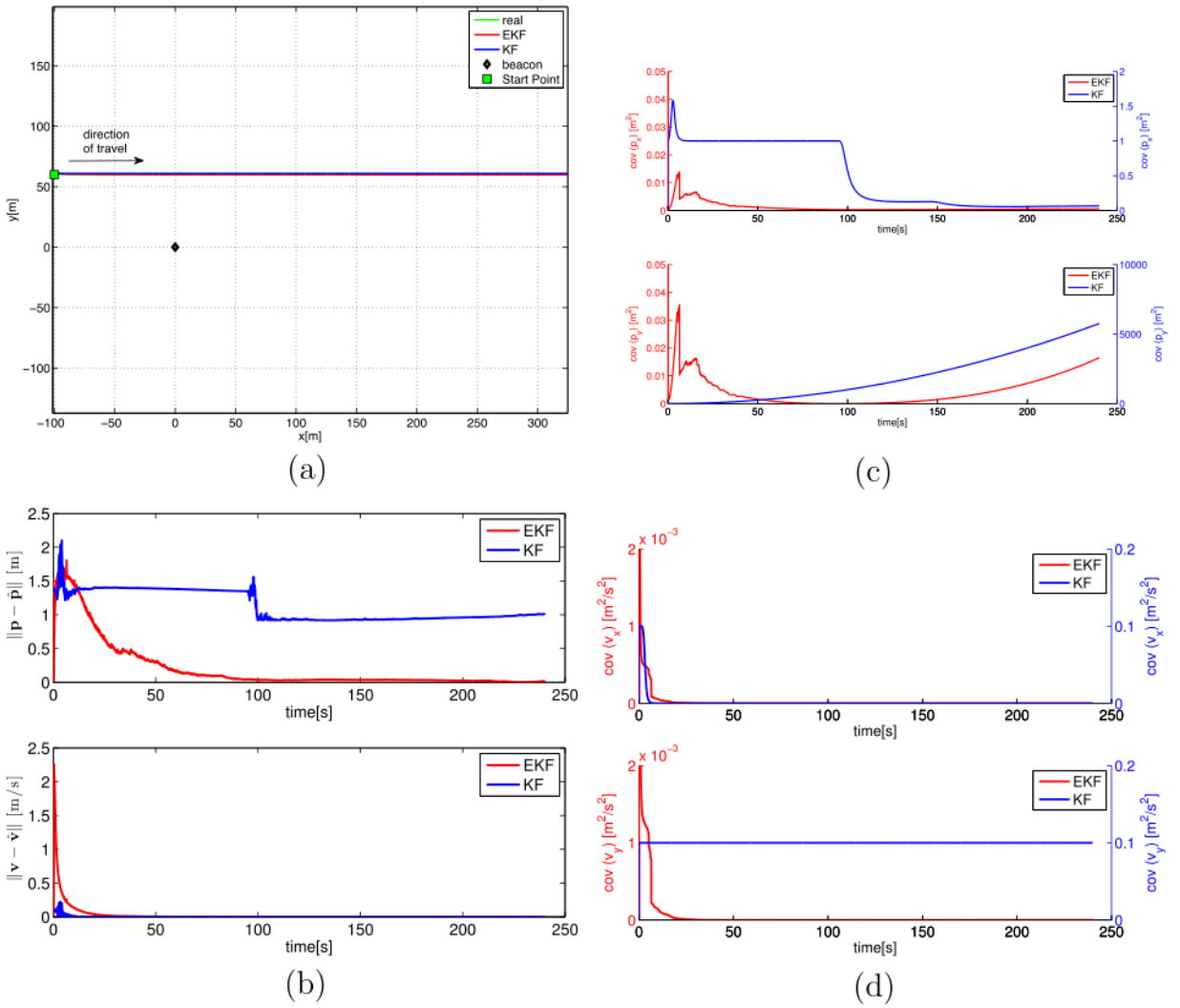

Fig. 1. Straight line motion in 2D: (a) trajectory, (b) norm of estimation errors, (c) position covariances and (d) velocity covariances.

column rank. This allows to overcome the rank deficiency issue in 3D case when only range measurements are available. Note that, if the circular motion is in the same plane of the beacon (i.e. $q_z = 0$), then the local weak observability condition is not satisfied. Of course, any 3D circular trajectory is not globally observable due to the presence of parallel circular trajectories with equal velocity and range from the beacon (with $q_{z,2} = -q_z$). This is also confirmed by the rank deficiency of the corresponding observability Gramian.

On the other hand, three-dimensional trajectories sufficiently exciting along each axis, already observable with range only measurements, continue to preserve their global observability in presence of a DVL. An example is the trajectory consisting in a circular motion in the (x, y) plane and a sinusoidal motion along the z axis.

The concatenation of three-dimensional trajectories sufficiently exciting and straight motions results in globally observable trajectories.

The results of this observability analysis are summarized in Table 2.

6.3. Remark: presence of unknown ocean current

The effect of the presence of DVL measurements can be extended to the case where the vehicle is subject to a constant, and unknown ocean current. In the literature, the presence of unknown ocean current in first order AUV kinematic models has been addressed, by example, in Scherbatyuk (1995), Gadre and Stilwell (2005), Batista et al. (2011b, 2011a), Viegas et al. (2012), Crasta et al. (2014), Crasta et al. (2015), Bayat et al. (2016).

In particular, papers Viegas et al. (2012) and Crasta et al. (2014, 2015) focus on the analysis of single beacon observability with range measurements only. Viegas et al. (2012) proposes cooperative navigation solutions for an intervention AUV working in tandem with an Autonomous Surface Craft (ASC). A sufficient condition for observability and a method for designing state observers with globally asymptotically stable error dynamics are presented. In Crasta et al. (2014, 2015) the authors introduce weaker definitions of observability that are akin to those proposed by Hermann and Krener (1977), but reflect the fact that they consider specific kinds of maneuvers in 3D. They study the observability properties of a 3D kinematic model of an AUV undergoing trimming trajectories; moreover, they give a complete characterization of the sets of states that are indistinguishable from a given initial state.

The work in Bayat et al. (2016) addresses the problem of range-based simultaneous AUV/multibeacon localization in the presence of ocean currents considering the presence of a depth sensor. Conditions are derived under which it is possible to reconstruct the initial

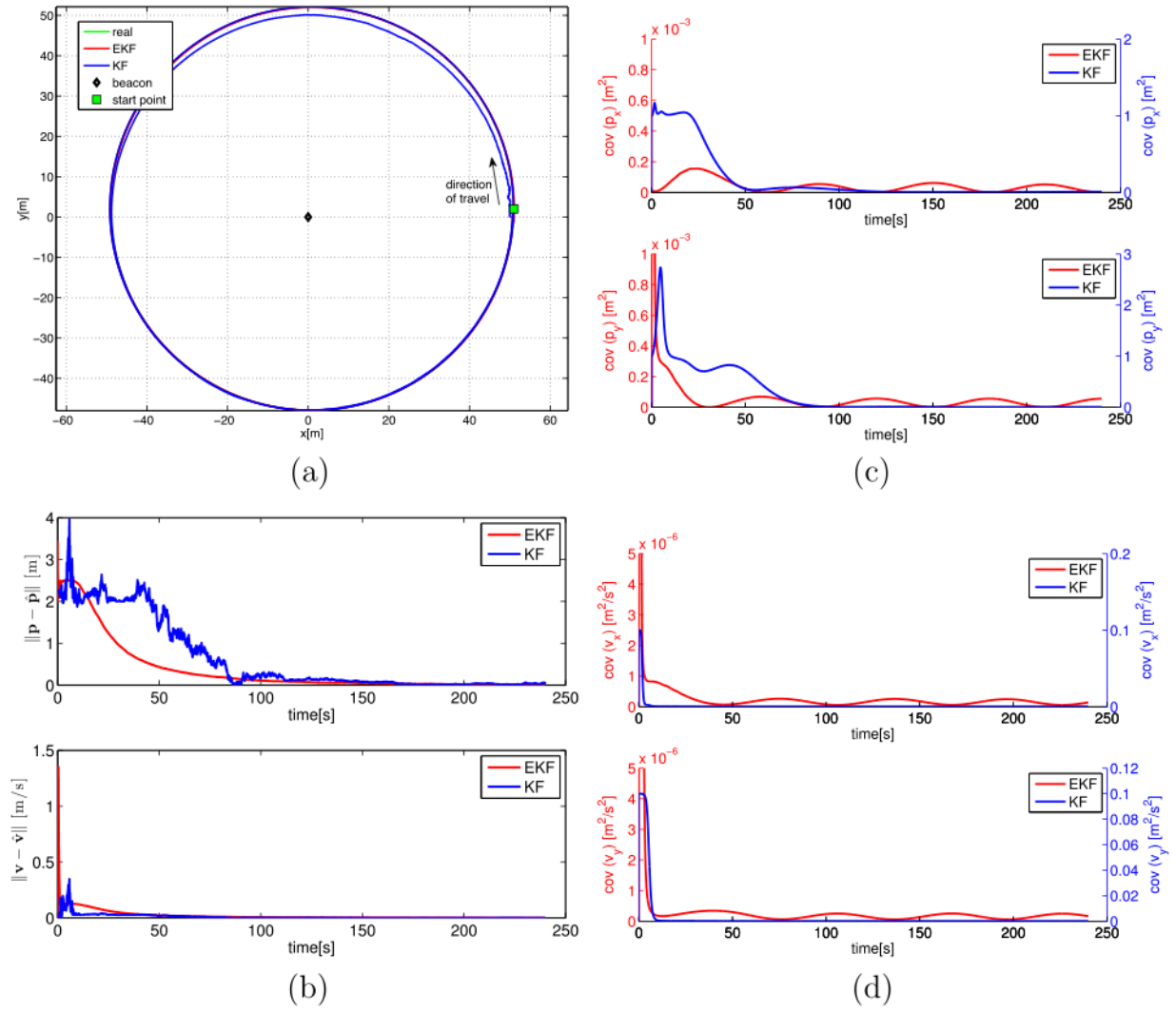

Fig. 2. Circular motion in 2D: (a) trajectory, (b) norm of estimation errors, (c) position covariances and (d) velocity covariances.

condition of the system under study. A multiple-model observer is proposed for simultaneous AUV and beacon localization.

In Batista et al. (2011b) necessary and sufficient conditions for the observability of the nonlinear system are derived considering the presence of velocity measurements; moreover, the nonlinear system is represented as an LTV system that is appropriate for state estimation of the nonlinear range based system.

The works in Scherbatyuk (1995), Gadre and Stilwell (2005) and Batista et al. (2011a) address the single beacon observability analysis considering both depth and velocity measurements. In Scherbatyuk (1995) a localization algorithm based on a least squares root method is presented. In Gadre and Stilwell (2005), unknown constant ocean currents are included into the state vector and the observability of the resulting model is studied using the same procedure in Gadre and Stilwell (2004): the results are local in nature. Batista et al. (2011a) focuses on the observability of linear motion quantities (position, linear velocity, linear acceleration, and accelerometer bias). They present necessary and sufficient conditions for the observability of these variables in 3D.

In the section below, the local weak and global observability analysis in 3D case for a double integrator system in presence of ocean currents considering only range and DVL readings (without using depth measurements) is addressed.

The state equations of the kinematic vehicle model are given by Eqs. (28)–(30) and can be represented in the state space as follows:

$$\dot{\mathbf{x}} = \begin{bmatrix} 0_{n\times n} & I_{n\times n} & I_{n\times n} \\ 0_{n\times n} & 0_{n\times n} & 0_{n\times n} \\ 0_{n\times n} & 0_{n\times n} & 0_{n\times n} \end{bmatrix} \mathbf{x} + \begin{bmatrix} 0_{n\times n} \\ I_{n\times n} \\ 0_{n\times n} \end{bmatrix} \mathbf{u}, \tag{47}$$

where $\mathbf{x} = (\mathbf{p}^\top, \mathbf{v}^\top, \mathbf{v}_f^\top)^\top \in \mathbb{R}^{3n}$ is the system state. The output equations depend on the specific acquisition through the DVL. Indeed, depending on the vehicle altitude and on the DVL range, a DVL unit can either measure the vehicle velocity with respect to the sea bottom ($\mathbf{v} + \mathbf{v}_f$) or with respect to the water column ($\mathbf{v}$). The former will be referred to as DVL in bottom tracking mode (or DVL bottom lock), the latter as DVL in water profiling mode. By combining the DVL measurements and the range measurements, the output equation takes the form in (48) or (49) for DVL in bottom tracking mode or in water profiling mode, respectively.

$$\mathbf{y} = \begin{bmatrix} y_1 \\ \mathbf{y}_b \end{bmatrix} = \begin{bmatrix} \frac{1}{2}\mathbf{p}^\top \mathbf{p} \\ \mathbf{v} + \mathbf{v}_f \end{bmatrix} \text{ (DVL in bottom tracking mode)}, \tag{48}$$

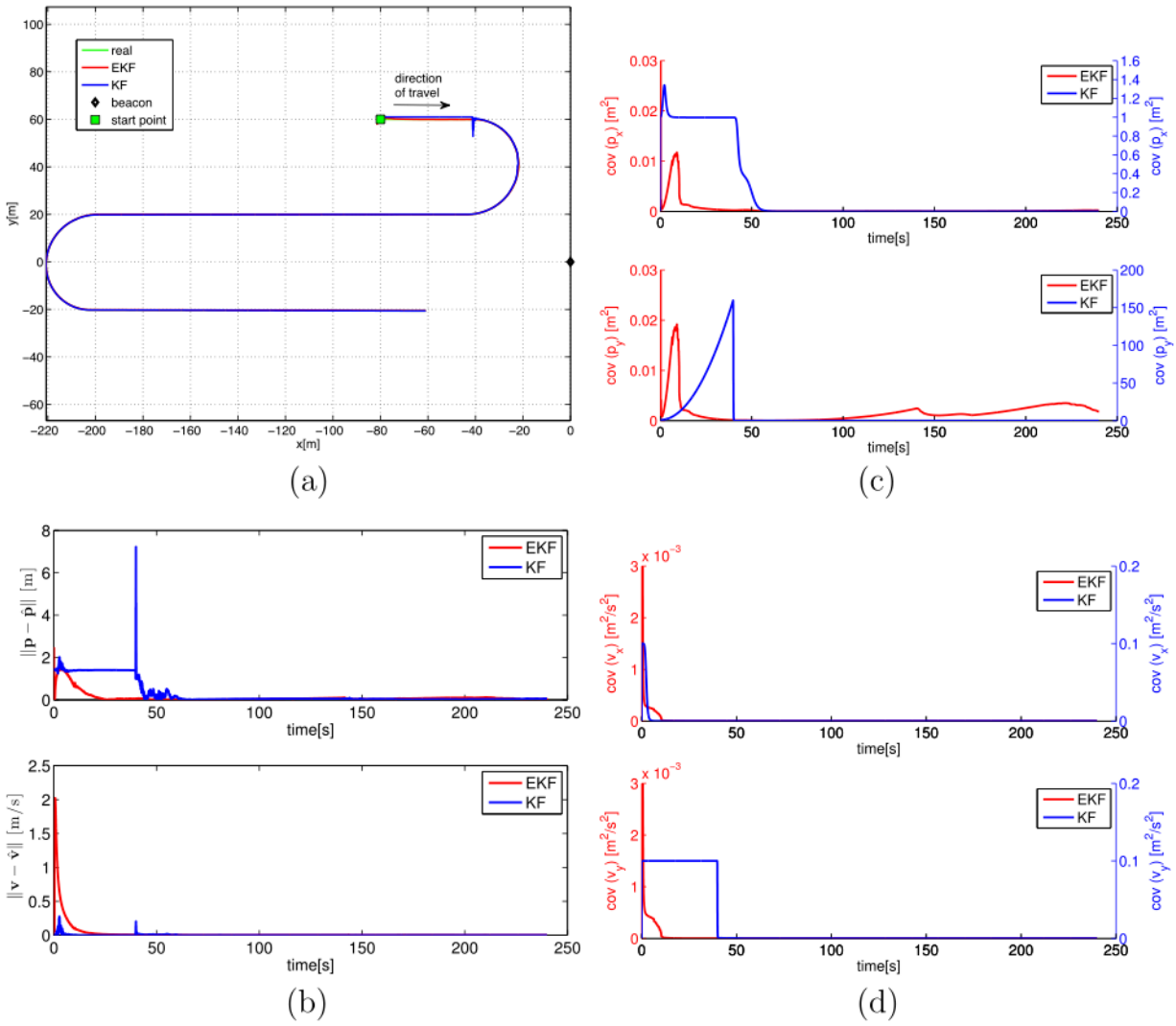

Fig. 3. Lawn mowing motion in 2D: (a) trajectory, (b) norm of estimation errors, (c) position covariances and (d) velocity covariances.

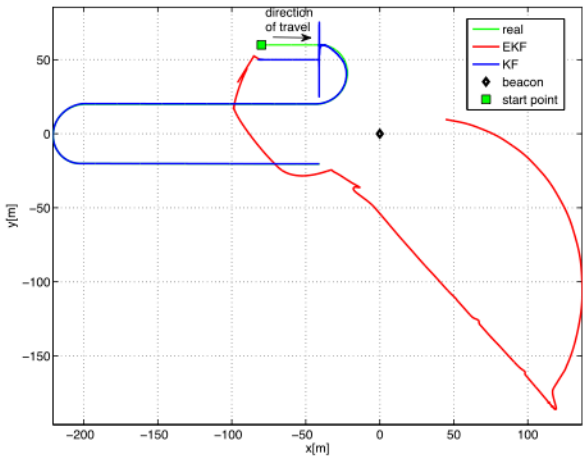

Fig. 4. Lawn mowing motion in 2D from a initial condition far from true value.

$$\mathbf{y} = \begin{bmatrix} y_1 \\ \mathbf{y}_w \end{bmatrix} = \begin{bmatrix} \frac{1}{2}\mathbf{p}^\top \mathbf{p} \\ \mathbf{v} \end{bmatrix} \text{ (DVL in water profiling mode).} \tag{49}$$

Consequently, the local weak observability matrix takes the form of O_b or O_w in (50), respectively.

$$O_b = \begin{bmatrix} \mathbf{p}^\top & 0_{1\times n} & 0_{1\times n} \\ (\mathbf{v}+\mathbf{v}_f)^\top & \mathbf{p}^\top & \mathbf{p}^\top \\ \mathbf{u}^\top & 2(\mathbf{v}+\mathbf{v}_f)^\top & 2(\mathbf{v}+\mathbf{v}_f)^\top \\ 0_{1\times n} & 3\mathbf{u}^\top & 3\mathbf{u}^\top \\ 0_{1\times n} & 0_{1\times n} & 0_{1\times n} \\ \vdots & \vdots & \vdots \\ 0_{n\times n} & I_{n\times n} & I_{n\times n} \\ 0_{n\times n} & 0_{n\times n} & 0_{n\times n} \\ \vdots & \vdots & \vdots \end{bmatrix},$$

$$O_w = \begin{bmatrix} \mathbf{p}^\top & 0_{1\times n} & 0_{1\times n} \\ (\mathbf{v}+\mathbf{v}_f)^\top & \mathbf{p}^\top & \mathbf{p}^\top \\ \mathbf{u}^\top & 2(\mathbf{v}+\mathbf{v}_f)^\top & 2(\mathbf{v}+\mathbf{v}_f)^\top \\ 0_{1\times n} & 3\mathbf{u}^\top & 3\mathbf{u}^\top \\ 0_{1\times n} & 0_{1\times n} & 0_{1\times n} \\ \vdots & \vdots & \vdots \\ 0_{n\times n} & I_{n\times n} & 0_{n\times n} \\ 0_{n\times n} & 0_{n\times n} & 0_{n\times n} \\ \vdots & \vdots & \vdots \end{bmatrix}. \tag{50}$$

Interestingly, in the 2D case the matrix O_b in (50) (bottom tracking mode) is rank deficient along both classes of trajectories, straight and circular. On the other hand, with the DVL in water profiling mode the matrix O_w in (50) has full column rank along both classes of trajectories

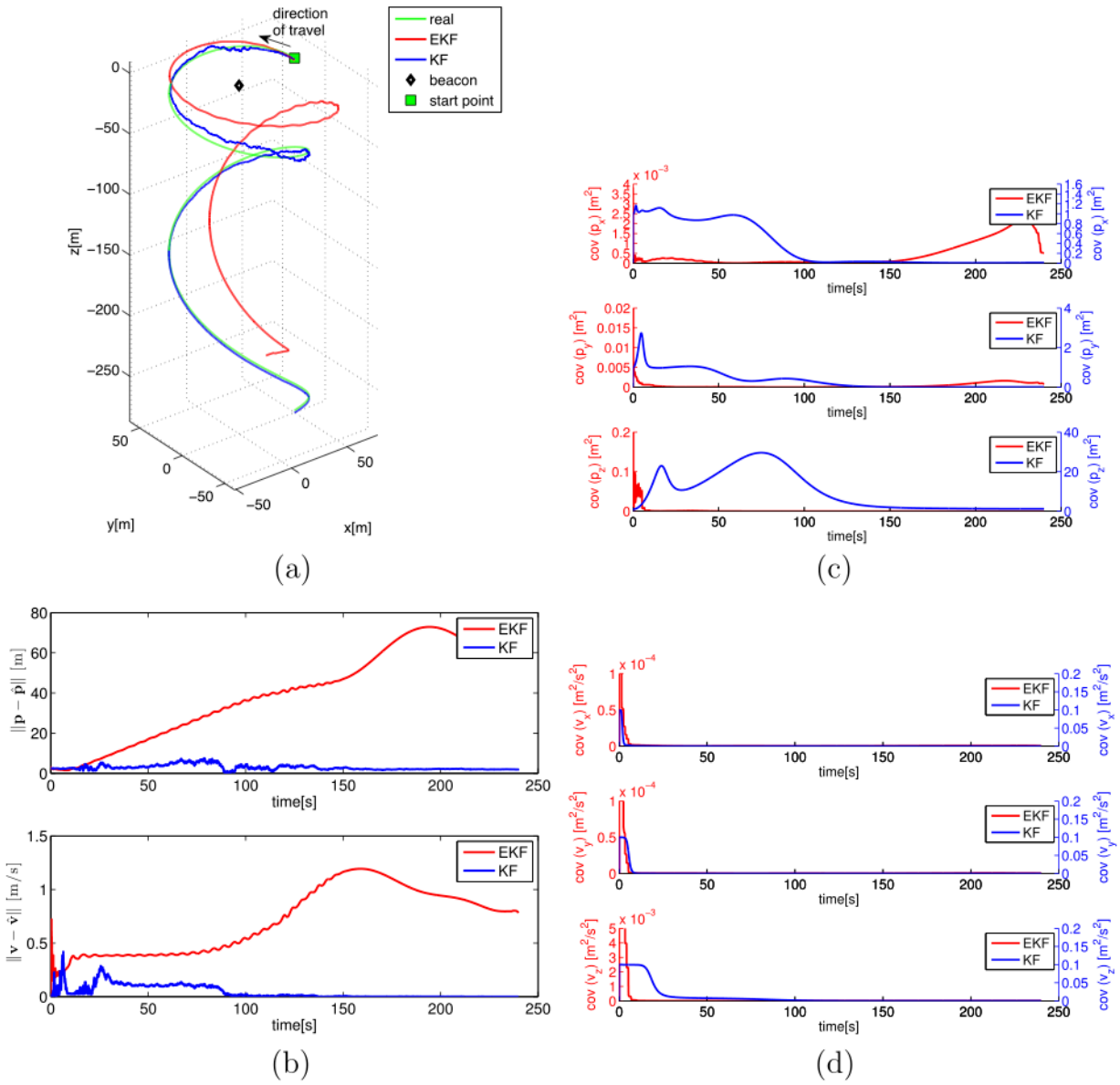

Fig. 5. Circular motion in 3D with a straight motion along the z axis: (a) trajectory, (b) norm of estimation errors, (c) position covariances and (d) velocity covariances.

granting local weak observability. This allows to estimate the complete state of the system, i.e. the position and velocity of the vehicle, and the velocity of the ocean current. With reference to the 3D case, it is worth highlighting that the observability matrices O_b and O_w have only 7 not null rows, implying that the local weak observability condition (rank $(O) = 3\,n = 9$) is never satisfied. Of course, integrating the measurements with a depth sensor, the 3D observability analysis will reduce to the 2D case, preserving the local weak observability when the DVL is in water profiling mode. This remark suggests that, if possible, it is convenient to use the DVL in water profiling mode rather than in bottom tracking mode.

The global observability analysis can be performed on the LTV representation of the nonlinear system (47)–(48) or (47)–(49) (obtained through the *state augmentation* method). In such a case the observability Gramian for the considered classes of motions (2D and 3D) associated to both DVL configurations is rank deficient and leads to a violation of the observability condition.

The results of this observability analysis are summarized in Table 3.

7. Numerical validation

Several numerical simulations have been performed to validate the proposed observability analysis. With reference to the model in Eqs. (4)–(5), let's assume that it is discretized with a sampling time T_s and affected by zero mean, mutually independent, state and output disturbances γ and ϵ with covariances Q and R respectively. While the discretization time step T_s needs to satisfy Shannon's Theorem sampling constraint and is hence bound to be rather small, notice that some AUV sensors provide rather low update rates. Indeed while T_s is reasonably bound to be lower than 0.1 [s], the update period of an underwater acoustic range device can be in the order of 1 [s] or even larger. Given that the major objective of the paper is to evaluate the theoretical and methodological aspects of the proposed approaches, rather than technological issues, two sets of simulation results are illustrated: case *A* and case *B*. In the first (covering most of the situations discussed in the paper), the range measurements are assumed to be acquired with the same sampling time $T_s = 0.01$ [s] used for the evolution of the model: this allows to validate the presented continuous time observability analysis through the simplest possible discretization schema without jeopardiz-

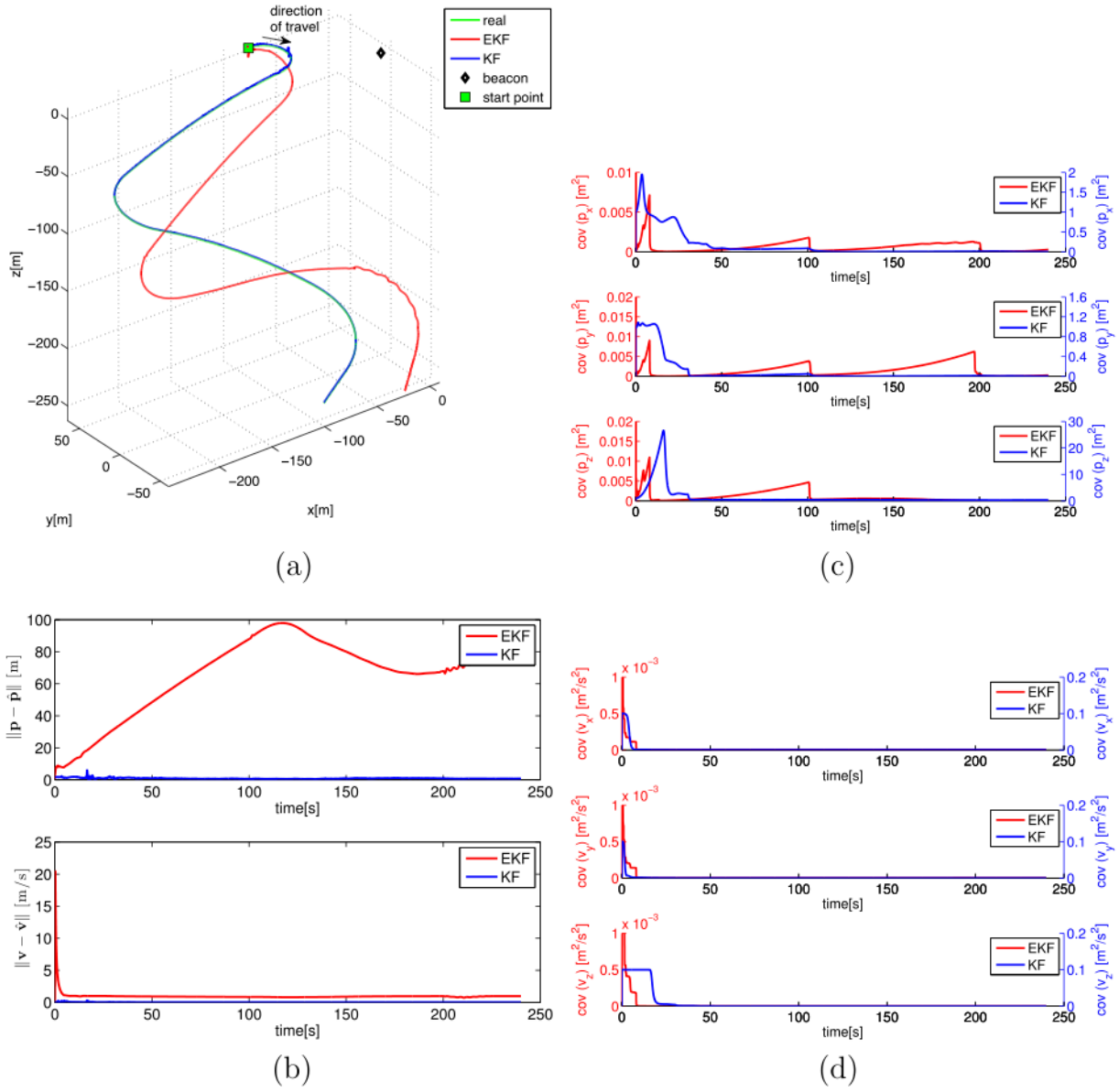

Fig. 6. Lawn mowing motion in 3D with a straight motion along the z axis: (a) trajectory, (b) norm of estimation errors, (c) position covariances and (d) velocity covariances.

ing the observability validation analysis. After illustrating this first set (case A) of numerical validation results, a second simulation example (case B) is reported where the range measurement is (more realistically) acquired at 0.1 [Hz] while the other sensors and the discrete model update frequency are kept at 100 [Hz].

Two different kinds of filters are implemented to estimate the AUV position and velocity: an EKF based on the nonlinear system in (4)–(5) and a KF based on the equivalent linear system in (24).

Within case A (i.e. with the range measurement acquired every T_s = 0.01 [s] being T_s the discretization sampling time), two sets of numerical simulations are considered: the first one in a 2D case and the second one in a 3D case. Common to all the simulations is the use of the covariance for the range measurements $R = (0.1\ [\mathrm{m}])^2$, the state noises covariances associated with the two filters

$$Q_{EKF} = (\mathrm{diag}([10^{-3}T_s I_{1\times n},\ 10^{-3}T_s I_{1\times n}]))^2,$$
$$Q_{KF} = (\mathrm{diag}([10^{-3}T_s I_{1\times n},\ 10^{-3}T_s I_{1\times n},\ 10^{-6},\ 10^{-6}]))^2$$

and the initial estimation error covariance for the two filters

$$P_{EKF} = \mathrm{diag}([I_{1\times n},\ 0.1\ I_{1\times n}]),$$
$$P_{KF} = \mathrm{diag}([I_{1\times n},\ 0.1\ I_{1\times n},\ 1,\ 1])$$

with proper units (i.e. [m^2] for position variables and [(m/s)^2] for velocity variables). Moreover, both filters are initialized with a same initial position error greater than the accuracy of the range measurements.

7.1. Case A: 2D model

The first numerical simulation is a 2D straight line motion parallel to the x axis. The trajectory is reported in Fig. 1(a) where the EKF estimate is depicted in red and the KF estimate in blue. The filters are initialized with a position $\hat{\mathbf{p}}_0 = (-101, 61)^\top$ [m] and a velocity $\hat{\mathbf{v}}_0 = (0.2, 0)^\top$ [m/s] as opposed to the real initial values $\mathbf{p}_0 = (-100, 60)^\top$ [m], $\mathbf{v}_0 = (0.1, 0)^\top$ [m/s]. The norm of the estimation errors, the position and velocity covariances of the two filters are also shown in Fig. 1(b)–(d). As expected, the original nonlinear system along the states of this trajectory is locally weakly observable, so the EKF properly initialized converges to the true state. On the other side, the LTV system does not satisfy the observability condition, due to the

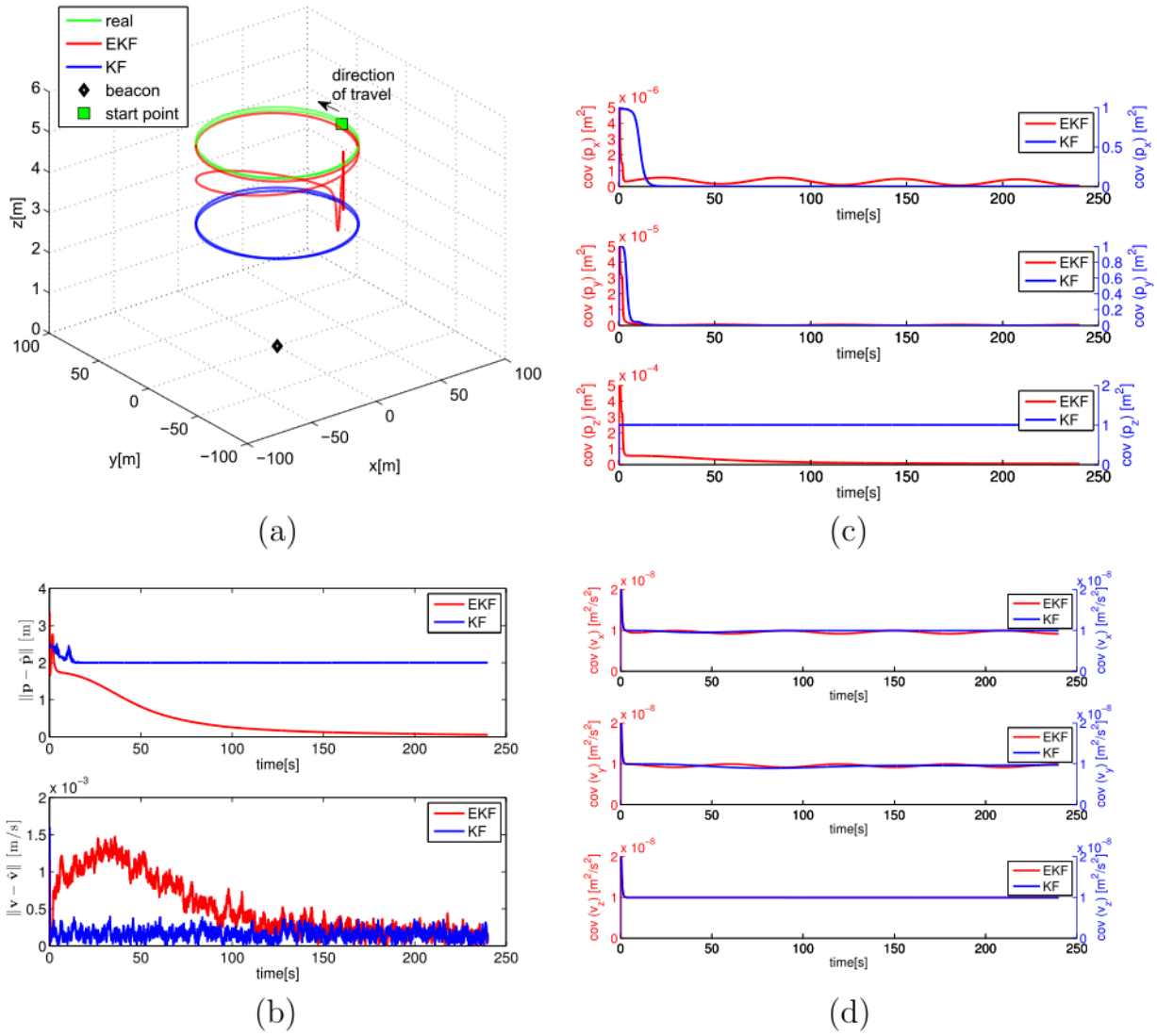

Fig. 7. Circular motion in 3D out of the plane of the beacon with DVL measurements: (a) trajectory, (b) norm of estimation errors, (c) position covariances and (d) velocity covariances.

fact that the y component is not sufficiently excited. Indeed, in this case the input along the y axis is null ($u_y = 0$), so the y component of the displacement $\mathbf{d}(t, t_0)$ in (15) is zero leading to a null row in the observability Gramian in (25), (27). As a result, the covariance on p_y is very large, the filter does not converge to the true state and there is a non zero estimation error.

With reference to radial trajectories (i.e. 2D straight line motion passing through the origin where the beacon is located), in Section 5.1 it is shown that they do not satisfy the local weak observability condition. Also the observability Gramian associated to the LTV system is not full rank, so a possible KF will not converge to the true state. Numerical examples with radial trajectories are not reported for the sake of brevity.

The next numerical experiment is related to the 2D circular motion. From the observability analysis presented, this class of motion is both locally weakly and globally observable. The estimations related to such a trajectory are illustrated in Fig. 2(a). The filters are initialized with a position $\hat{\mathbf{p}}_0 = (50, 0)^\top$ [m] and a velocity $\hat{\mathbf{v}}_0 = (0, 2.6)^\top$ [m/s] as opposed to the real initial values $\mathbf{p}_0 = (51, 2)^\top$ [m], $\mathbf{v}_0 = (0, 2.6)^\top$ [m/s]. The norm of the estimation errors, the position and the velocity covariances associated with the two filters are also shown in Fig. 2(b)–(d). As expected, both filters converge to the real state.

Finally, a 2D lawn mowing trajectory is considered through the concatenation of straight line trajectories with circular trajectories (globally observable) as in Fig. 3. The filters are initialized with a position $\hat{\mathbf{p}}_0 = (-81, 61)^\top$ [m] and a velocity $\hat{\mathbf{v}}_0 = (0, 0)^\top$ [m/s] as opposed to the real initial values $\mathbf{p}_0 = (-80, 60)^\top$ [m], $\mathbf{v}_0 = (0, 0)^\top$ [m/s]. Note that the states along the whole trajectory are locally weakly observable; indeed, the EKF estimation error converges to zero. On the other hand, in the first straight line motion, where the observability Gramian of the LTV system with augmented state is rank deficient, the KF exhibits a non zero estimation error. Such an error decreases only once the LTV system is observable, i.e. during the circular motion. As illustrated in Fig. 3(c), in this first part of trajectory the position covariance along the y axis increases significantly since the y component is not excited. When the LTV system becomes observable, there is a transient phase where the filter starts to correct the estimate leading to a final convergence. Interestingly, in the next straight line motions the filter preserves its convergence, in fact, the observability condition is still satisfied. This confirms that, referring to the LTV system with augmented state, the concatenation of an unobservable trajectory (or a trajectory not satisfying the observability condition) after an observable one, still results in an observable motion.

A further simulation for the same case has been performed starting from a large initial estimation error, i.e. $\hat{\mathbf{p}}_0 = (-81, 50)^\top$ [m]. In such a condition, the EKF does not converge to the true state, whereas the KF estimate based on the LTV system with *augmented state* converges to the true state even if initialized far from the real state. The resulting

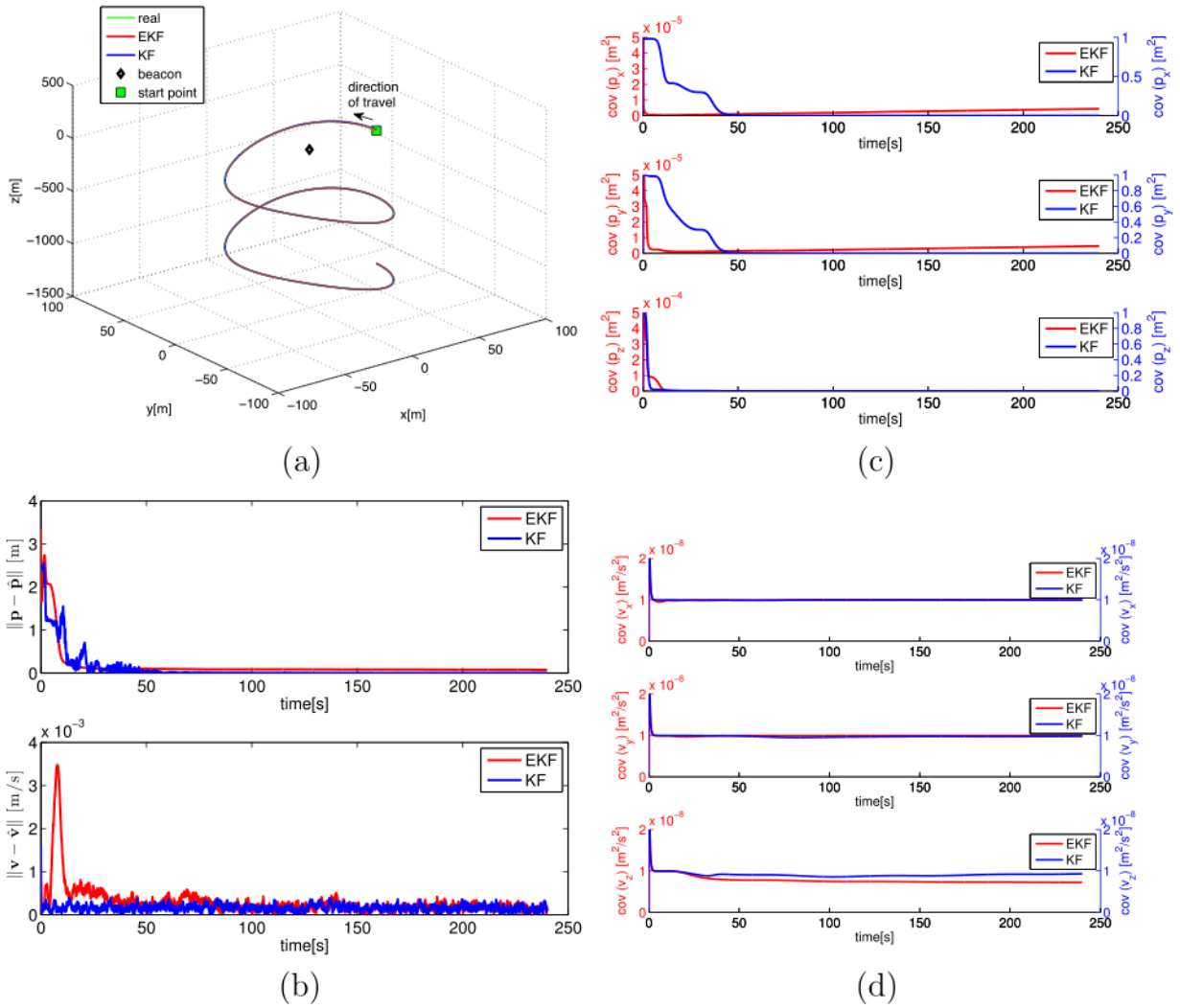

Fig. 8. Circular motion in 3D with exciting motion along the z axis with DVL measurements: (a) trajectory, (b) norm of estimation errors, (c) position covariances and (d) velocity covariances.

trajectories estimated through the EKF and KF are reported in Fig. 4.

7.2. Case A: 3D model

The numerical validations in the 3D case refers to circular motions and lawn mowing motions in the (x, y) plane as in the 2D case combined with a straight motion along the z axis. Fig. 5(a) reports the 3D trajectories obtained from the following initial position and velocity estimates $\hat{\mathbf{p}}_0 = (50, 0, 5)^T$ [m], $\hat{\mathbf{v}}_0 = (0, 2.6, -0.01)^T$ [m/s] as opposed to the real initial state $\mathbf{p}_0 = (51, 1, 4)^T$ [m], $\mathbf{v}_0 = (0, 2.6, -0.01)^T$ [m/s]. The norm of the estimation errors, the position and velocity covariances associated with the EKF and KF filters are also shown in Fig. 5(b)–(d). As noted, in the 3D case the local weak observability rank condition is not satisfied. The numerical experiment highlights that the EKF estimate does not converge to the true state even if initialized close to the true state. Moreover, even though the covariances of the state are not large, the position estimation error is significant. Contrary to the EKF, it is worth highlighting that the KF estimate is characterized by a transient phase where the state covariances and the errors are large, but once the LTV system satisfies the observability condition, they rapidly decrease.

Finally, a 3D lawn mowing trajectory has been considered. The results are similar to the previous case. The estimated trajectories, the norm of the estimation errors and the position and velocity covariances associated with the EKF and KF filters are shown in Fig. 6. The filters are initialized with a position $\hat{\mathbf{p}}_0 = (-81, 61, 6)^T$ [m] and a velocity $\hat{\mathbf{v}}_0 = (2, 0, 0)^T$ [m/s] as opposed to the real initial values $\mathbf{p}_0 = (-80, 60, 5)^T$ [m] and $\mathbf{v}_0 = (2, 0, 0)^T$ [m/s]. As noted in the previous simulation, the EKF estimate does not converge to the true state even if the state covariances are small. On the other hand, the KF based on the LTV system with augmented state converges to the real state even if after a transient phase. The state covariances that increase in the transient, rapidly converge to zero once the system satisfies the observability condition. It is worth noting that in all the described simulations the position covariance along the z axis is greater than the other axes, this is due to the fact that the trajectory along the z axis is not so rich, even though it is rich enough to make the observability rank condition satisfied.

A last validation has been performed considering the presence of velocity measurements. Assuming to acquire the velocity through a DVL unit, a covariance for the velocity measurements $R_{DVL} = (10^{-6})\text{diag}([1, 1, 1])$ $[(\text{m/s})^2]$ has been considered. The effect of DVL measurements have a significant impact on the local weak observability of 3D motions. In particular, a 3D circular motion out of the plane of the beacon has been simulated. Fig. 7 reports the 3D trajectories obtained from the following initial position and velocity estimates $\hat{\mathbf{p}}_0 = (51, -1, 3)^T$ [m], $\hat{\mathbf{v}}_0 = (0, 2.6, 0)^T$ [m/s] as opposed to the real initial state $\mathbf{p}_0 = (50, 0, 5)^T$ [m], $\mathbf{v}_0 = (0, 2.6, 0)^T$ [m/s]. The norm of the estimation errors, the position and velocity covariances associated with the EKF and KF filters are also shown in Fig. 7.

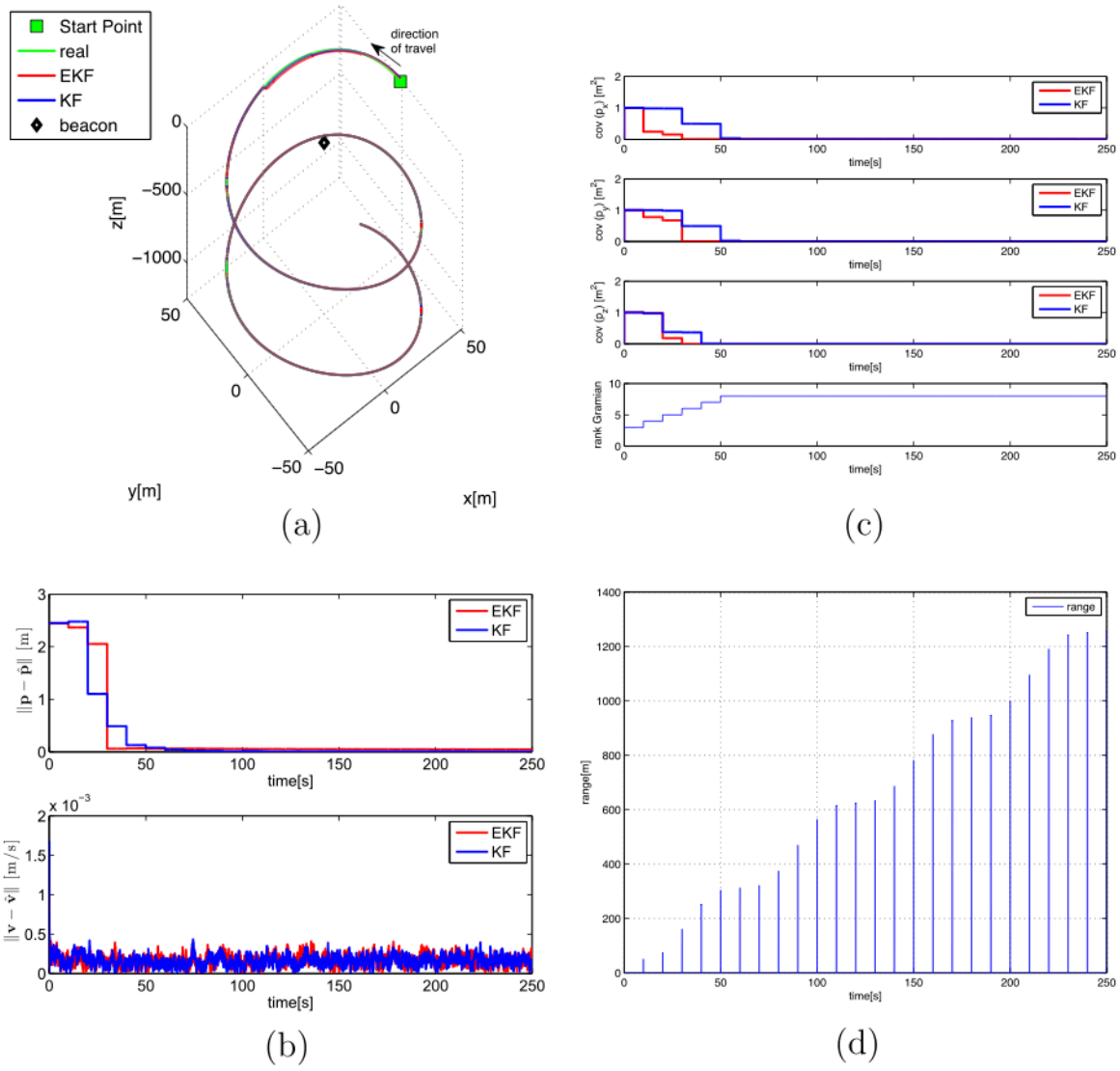

Fig. 9. Circular motion in 3D with exciting motion along the z axis with DVL measurements: (a) trajectory, (b) norm of estimation errors, (c) position covariances and rank of Gramian and (d) low-frequency range measurements.

As expected, the EKF estimate converges to the true state thanks to the local weak observability granted by the integration of DVL measurements. Whereas, the KF estimate does not converge to the true state due to the global unobservability of such trajectory, as highlighted in Section 6.2. Even in presence of DVL measurements, the trajectory should be sufficiently exciting along each axis in order to be globally observable. Thus, a circular motion in the (x, y) plane with an exciting motion along the z axis has been simulated. Refer to the Fig. 8 for the 3D trajectory, the norm of the estimation errors, the position and velocity covariances associated with the EKF and KF filters. In this case both filters converge to the true state. Indeed, such a trajectory is both locally weakly and globally observable.

7.3. Case B: low-frequency range measurements

In real world operations, the AUVs commonly get measurements of the range to the beacons by measuring the time of flight of acoustic signals. Thus, due to the limited bandwidth of the underwater acoustic link, and due to the constraint for an AUV to access an acoustic communication network on a time division base with possible other nodes, it may result that the AUV is able to get range measurements at a frequency much lower than that of the other sensors used for the navigation, as INS or DVL. This section shows the results of a numerical case study where the range measurements have been under sampled.

In particular, Fig. 9 shows the results of the execution of a mission analogous to that reported in Fig. 8 where, here, the range measurements are acquired by the AUV with a frequency of 0.1 Hz. Thus, in both the Kalman Filter for the system with augmented state and in the Extended Kalman Filter for the non-linear system, the prediction step and the correction step relative to all the other sensors except the ranges were performed with a frequency of 100 Hz, while the correction with the range measurement was performed with a frequency of 0.1 Hz.

Fig. 9 shows: a) the real and the estimated 3D trajectory; b) the position covariance associated with the EKF and KF filters and the rank of the Gramian relative to the system with augmented state; c) the norm of position and velocity errors; d) the range measurements. Even in this case both filters converge to the true state , although at a lower rate due to the limited update frequency of the range measurements. From Fig. 9(b), it is also worth noting that the augmented system needs a set of range acquisitions in order to get a full rank Gramian matrix.

8. Conclusions

A range-based observability analysis has been presented for a 2D

and 3D vehicle modeled as a double integrator: both local weak observability and global observability properties have been discussed resorting to the tools of differential algebraic geometry and LTV systems theory. The results of the observability analysis have been validated and confirmed through a set of numerical simulations. While most of the illustrated simulations aim at validating the observability results and refer to the nominal model where range and other navigation sensors are acquired at the same sampling time used to integrate the system model, the more realistic case where range is acquired at a much lower frequency is also (successfully) validated numerically. These simulation results suggest that the proposed approach can be adopted in practice.

When the system is locally weakly observable along a trajectory an EKF estimator can be designed: being its convergence properties only local, the filter must be properly initialized to avoid the divergence of the estimation error. Unfortunately local weak observability is never satisfied in the 3D case. On the other side, when the system trajectories are globally observable for the LTV system a KF estimator can be adopted to estimate the state of the original nonlinear system: this solution guarantees global convergence although numerical simulations reveal that the estimate covariance matrix has larger norm with respect to the EKF counterpart. This can be at least partially explained by the fact that the LTV system has larger dimension with respect to the linearized system used to implement the EKF.

Moreover, the study of the effect of additional sensors as a DVL or a depth sensor on observability has also been addressed revealing that, when possible, it is convenient to use the DVL unit in water profiling mode. The analysis is completed with brief remarks on the state estimation in presence of constant, and unknown ocean currents. Indeed the velocity of the ocean current can be estimated through an EKF filter only in case of 2D motions if measurements from range and DVL in water profiling mode are available.

At last, note that the described approach can be extended to the case of multi-vehicle navigation: in particular, relative localization can be achieved when a vehicle has access to the range from another one and they share knowledge of their inputs. Preliminary results relative to this problem have been addressed for different first order kinematics models in Parlangeli and Indiveri (2014, 2015), De Palma et al. (2015) and Parlangeli et al. (2012).

Acknowledgements

This work was partially supported by the European Union's Horizon 2020 research and innovation programme under the project WiMUST: Widely scalable Mobile Underwater Sonar Technology, Grant agreement no. 645141 (call H2020 ICT-23-2014 Robotics).

References

Arrichiello, F., Heidarsson, H., Sukhatme, G., 2012. Opportunistic localization of underwater robots using drifters and boats. In: Proceedings 2012 IEEE International Conference on Robotics and Automation. St Paul, MN, pp. 5307–5314. http://dx.doi.org/http://dx.doi.org/10.1109/ICRA.2012.6224733.

Arrichiello, F., Antonelli, G., Aguiar, A., Pascoal, A., 2013. An observability metric for underwater vehicle localization using range measurements. Sensors 13 (12), 16191–16215. http://dx.doi.org/10.3390/s131216191.

Arrichiello, F., De Palma, D., Indiveri, G., Parlangeli, G., 2015. Observability analysis for single range localization. In: Proceedings of MTS/IEEE Oceans'15. Genova, Italy, pp. 1–10. http://dx.doi.org/10.1109/OCEANS-Genova.2015.7271684.

Bahr, A., Leonard, J.J., Fallon, M.F., 2009. Cooperative localization for autonomous underwater vehicles. Int. J. Robot. Res. 28 (6), 714–728. http://dx.doi.org/10.1177/0278364908100561.

Batista, P., Silvestre, C., Oliveira, P., 2011a. On the observability of linear motion quantities in navigation systems. Syst. Control Lett. 60 (2), 101–110. http://dx.doi.org/10.1016/j.sysconle.2010.11.002.

Batista, P., Silvestre, C., Oliveira, P., 2011b. Single range aided navigation and source localization: observability and filter design. Syst. Control Lett. 60, 665–673. http://dx.doi.org/10.1016/j.sysconle.2011.05.004.

Bayat, M., Crasta, N., Aguiar, A., Pascoal, A., 2016. Range-based underwater vehicle localization in the presence of unknown ocean currents: theory and experiments. Control Syst. Technol. IEEE Trans. 24 (1), 122–139. http://dx.doi.org/10.1109/TCST.2015.2420636, (PP (99)).

Crasta, N., Bayat, M., Aguiar, A.P., Pascoal, A.M., 2014. Observability analysis of 3D AUV trimming trajectories in the presence of ocean currents using single beacon navigation. In: Proceedings of the 19th IFAC World Congress, vol. 19. pp. 4222–4227. http://dx.doi.org/10.3182/20140824-6-ZA-1003.02263.

Crasta, N., Bayat, M., Aguiar, A.P., Pascoal, A.M., 2015. Observability analysis of 3D AUV trimming trajectories in the presence of ocean currents using range and depth measurements. Annu. Rev. Control 40, 142–156. http://dx.doi.org/10.1016/j.arcontrol.2015.09.009.

De Palma, D., Indiveri, G., Parlangeli, G., 2015. Multi-vehicle relative localization based on single range measurements. In: Proceedings of the 3rd IFAC Workshop on MultiVehicle System – MVS 2015, vol. 48. Genova, Italy, pp. 17–22. http://dx.doi.org/10.1016/j.ifacol.2015.06.457.

Fallon, M.F., Papadopoulos, G., Leonard, J.J., Patrikalakis, N.M., 2010. Cooperative AUV navigation using a single maneuvering surface craft. Int. J. Robot. Res. 29 (12), 1461–1474. http://dx.doi.org/10.1177/0278364910380760.

Gadre, A.S., Stilwell, D.J., 2004. Toward underwater navigation based on range measurements from a single location. In: Proceedings of IEEE International Conference on Robotics and Automation, 2004 (ICRA 2004), vol. 5. New Orleans, LA, USA, pp. 4472–4477. http://dx.doi.org/10.1109/ROBOT.2004.1302422.

Gadre, A., Stilwell, D., 2005. Underwater navigation in the presence of unknown currents based on range measurements from a single location. In: Proceedings of the 2005 American Control Conference. Portland, OR, pp. 565–661. http://dx.doi.org/10.1109/ACC.2005.1470032.

Hermann, R., Krener, A.J., 1977. Nonlinear controllability and observability. IEEE Trans. Autom. Control 22 (5), 728–740. http://dx.doi.org/10.1109/TAC.1977.1101601.

Hinson, B., Binder, M., Morgansen, K., 2013. Path planning to optimize observability in a planar uniform flow field. In: Proceedings of the American Control Conference (ACC), 2013. pp. 1392–1399. http://dx.doi.org/10.1109/ACC.2013.6580031.

Indiveri, G., Parlangeli, G., 2013. Further Results on the Observability Analysis and Observer Design for Single Range Localization in 3D. arXiv:1308.0517 [sc.RO], http://arXiv.org/abs/1308.0517.

Indiveri, G., De Palma, D., Parlangeli, G., 2016. Single range localization in 3-D: observability and robustness issues. IEEE Trans. Control Syst. Technol. 24 (5), 1853–1860. http://dx.doi.org/10.1109/TCST.2015.2512879.

Jazwinski, A.H., 2007. Stochastic Processes and Filtering theory. Courier Dover Publications, Mineola, New York.

Jouffroy, J., Reger, J., 2006. An algebraic perspective to single-transponder underwater navigation. In: Computer Aided Control System Design, 2006 IEEE International Conference on Control Applications, 2006 IEEE International Symposium on Intelligent Control. IEEE, pp. 1789–1794. http://dx.doi.org/10.1109/CACSD-CCA-ISIC.2006.4776912.

Kalman, R.E., 1960. Contributions to the theory of optimal control. In: Boletin de la Sociedad Matematica Mexicana, vol. 5. pp. 102–119.

Larsen, M., 2000. Synthetic long baseline navigation of underwater vehicles. In: Proceedings of the OCEANS 2000 MTS/IEEE Conference and Exhibition, vol. 3. Providence, RI, USA, pp. 2043–2050. http://dx.doi.org/10.1109/OCEANS.2000.882240.

Parlangeli, G., Indiveri, G., 2014. Single range observability for cooperative underactuated underwater vehicles. In: Proceedings of the 19th IFAC World Congress, vol. 19. pp. 5127–5138. http://dx.doi.org/10.3182/20140824-6-ZA-1003.02376.

Parlangeli, G., Indiveri, G., 2015. Single range observability for cooperative underactuated underwater vehicles. Annu. Rev. Control 40, 129–141. http://dx.doi.org/10.1016/j.arcontrol.2015.09.008.

Parlangeli, G., Pedone, P., Indiveri, G., 2012. Relative pose observability analysis for 3D nonholonomic vehicles based on range measurements only. In: Proceedings of the 9th IFAC Conference on Manoeuvring and Control of Marine Craft, MCMC 2012. Arenzano, GE, Italy, pp. 182–187. http://dx.doi.org/10.3182/20120919-3-IT-2046.00031.

Rugh, W.J., 1996. Linear System Theory. Prentice-Hall, New Jersey.

Scherbatyuk, A., 1995. The AUV positioning using ranges from one transponder LBL. In: OCEANS'95. MTS/IEEE. Challenges of Our Changing Global Environment. Conference Proceedings, vol. 3. San Diego, CA, USA, pp. 1620–1623. http://dx.doi.org/10.1109/OCEANS.1995.528728.

Silverman, L.M., Anderson, B.D., 1968. Controllability, observability and stability of linear systems. SIAM J. Control 6 (1), 121–130. http://dx.doi.org/10.1137/0306010.

Viegas, D., Batista, P., Oliveira, P., Silvestre, C., 2012. Position and velocity filters for intervention auvs based on single range and depth measurements. In: IEEE International Conference on Robotics and Automation (ICRA), 2012. pp. 4878–4883. http://dx.doi.org/10.1109/ICRA.2012.6224634.

Webster, S.E., Eustice, R.M., Singh, H., Whitcomb, L.L., 2012. Advances in single-beacon one-way-travel-time acoustic navigation for underwater vehicles. Int. J. Robot. Res. 31 (8), 935–949. http://dx.doi.org/10.1177/0278364912446166.